Cement and Concrete Research 47 (2013) 14–30

Contents lists available at SciVerse ScienceDirect

Cement and Concrete Research

journal homepage: http://ees.elsevier.com/CEMCON/default.asp

The di- and tricalcium silicate dissolutions

L. Nicoleau [a,*], A. Nonat [b], D. Perrey [b]

[a] BASF Research Construction Materials & Systems, BASF Construction Chemicals GmbH, 83308 Trostberg, Germany
[b] Institut Carnot de Bourgogne UMR5209 CNRS, 9 avenue Alain Savary, BP 47870, 21078 Dijon Cedex, France

ARTICLE INFO

Article history:
Received 19 August 2012
Accepted 29 January 2013

Keywords:
Kinetics (A)
Hydration (A)
Ca_3SiO_5 (D)
Ca_2SiO_4 (D)
CaO (D)

ABSTRACT

In this study, a specially designed reactor connected to an ICP spectrometer enabled the careful determination of the dissolution rates of C_3S, C_2S and CaO, respectively, over a broad range of concentration of calcium and silicates under conditions devoid of C–S–H. The kinetic laws, bridging the dissolution rates and the undersaturations, were obtained after extrapolation of rate zero allowing the estimation of the true experimental solubility products of C_3S ($K_{sp} = 9.6 \cdot 10^{-23}$), C_2S ($K_{sp} = 4.3 \cdot 10^{-18}$) and CaO ($K_{sp} = 9.17 \cdot 10^{-6}$). The latter are then compared to the solubilities calculated from the enthalpies of formation. We propose that the observed deviations result from the protonation of the unsaturated oxygen atoms present at the surface of these minerals. Hydration rates measured in cement pastes or in C_3S pastes are in excellent agreement with the kinetic law found in this study for C_3S under conditions undersaturated with respect to C–S–H.

1. Introduction

Tricalcium and dicalcium silicates (also known as C_3S and C_2S, respectively, in cement notation) represent about 75% of an ordinary Portland cement. They react with water through a dissolution–precipitation process, which leads to the precipitation, firstly, of calcium silicate hydrate, and secondly, of calcium hydroxide (Portlandite). Calcium silicate hydrate (so-called C–S–H) is the main hydrate responsible for the cohesion in cement binders [1] also investigations of the calcium silicates hydration in the last decades were of high importance in order to improve the properties of concrete. In general terms, we have to admit that the development of dissolution theories received significantly less attention in comparison with its counterpart, the crystal growth. In the field of cement, the nucleation and growth of C–S–H were comprehensively investigated whilst there are only few studies of the dissolution of C_3S and none on C_2S until today. Dissolution of calcium silicates was seldomly studied due to an experimental hurdle and also its quasi absence in nature. The experimental hurdle is connected to the much greater solubility of C_3S compared to C–S–H. Indeed, only a very tiny quantity of dissolved tricalcium silicate is needed for the precipitation of C–S–H to occur, which impedes a measurement of the solubility of C_3S under saturated conditions. This issue has therefore prevented the measurement of the solubilities of both these anhydrous calcium silicate phases until now. The lack of information about the dissolution behavior of C_3S/C_2S has consequently led to the proposition of various models describing their hydration based solely on the growth of C–S–H [2–5]. Unsurprisingly, it was recently demonstrated that the dissolution should be taken into account for correctly modeling the hydration of tricalcium silicate [6].

Contrary to these two anhydrous cement phases, natural silicates have been the object of thorough investigations regarding their mode of dissolution in order to predict the evolution of complex geochemical systems. In this quest, one requirement is to quantitatively predict the dissolution kinetics of minerals, hence the need for bridging thermodynamics and kinetics. The driving force for dissolution is undersaturation, i.e. the deviation between the solubility and the ion activity of constituents of the mineral in solution. Crystal dissolution (like its counterpart crystal growth) proceeds through the transport of water and dissolution products to and from the crystal surface where reactions occur. The dissolution is then the resulting process of interfacial reactions and all transport phenomena but the overall rate is always limited by the slowest event, i.e. either the transport or one of the surface reactions. In the possible event of a limitation by a reaction, it makes sense to consider the corresponding chemical equilibrium:

$$A_xB_y \leftrightarrows xA + yB \quad \Delta_{diss}G \tag{1}$$

and to calculate the deviation from equilibrium, i.e. the Gibbs free energy change

$$\Delta_{diss}G = \Delta_{diss}G^0 + RT\ln(A)^x(B)^y \tag{2}$$

where (A) and (B) are the activities of A and B in the solvent, R the gas constant and T the temperature.

The rate of dissolution should follow a general low such as:

$$Rate = k \cdot S_{reac}(t) \cdot f(\Delta G) \tag{3}$$

* Corresponding author. Tel.: +49 8621862734; fax: +49 862166502734.
E-mail address: luc.nicoleau@basf.com (L. Nicoleau).

0008-8846/$ – see front matter © 2013 Elsevier Ltd. All rights reserved.
http://dx.doi.org/10.1016/j.cemconres.2013.01.017

with k being the rate constant, S_{reac} the reactive surface area and f a priori unknown function of the free enthalpy. The plot of the interfacial experimental dissolution rates against the free enthalpy change over a very broad range of undersaturation generally leads to such a sigmoidal graph as represented in Fig. 1 [7–11] showing three different kinetic domains.

First developments related to dissolution kinetics were derived from the transition state theory (T.S.T.) developed by Eyring. The system has to overcome an energy barrier due to the formation of an activated complex. Considering that the rate-law is limited by this formation, the overall interfacial rate law may be written as follows [12,13]:

$$\text{Rate}_{\text{interfacial}} = A\cdot\left(1-\exp\left(\alpha\frac{\Delta G_{\text{diss}}}{RT}\right)\right) \quad (4)$$

where A and α are general constants, ΔG is the Gibbs free energy associated with the dissolution reaction, and R the gas constant. However, a true T.S.T. model implies ignoring all crystal surface features and considering an amorphous-like surface which is rarely the case in natural systems. With the law expressed above (Eq. (4)), it is not possible to correctly fit such an S-curve presented in Fig. 1. Despite the fact that a unique theoretical description of $f(\Delta G)$ over the entire range of ΔG is still under debate, we will strive to describe the curve in Fig. 1, starting and deviating from the equilibrium, from a phenomenological point of view:

Domain III: In this part, a slow evolution of the dissolution rate with the free enthalpy is usually observed. At the solubility equilibrium, $\Delta G = 0$, the rate is zero. The rate increases with the decrease of ΔG. When the free enthalpy is sufficiently low, smaller than ΔG_{crit} (see below), another mechanism occurs. Lasaga et al. [14] proposed that the dissolution occurs by step-waves emanating from surface defects. Train of steps originating at the outskirts of etch pits causes the retreat of the overall crystal surface layer by layer. This theory was developed as the counterpart of the B.C.F. (Burton–Cabrera–Frank) theory for the crystal growth. The defects outcropping at the surface, source of these stepwaves and thus of mass removal are preferential sites of dissolution if the free energy $\Delta G_{nucleation}(r)$ for the nucleation of a dissolution hole of radius r is reached:

$$\Delta G_{\text{nucleation}}(r) = \frac{\pi r^2\cdot h}{V_m}\left[\Delta G_{\text{diss}}^{\frac{1}{\nu}}\right] + 2\pi r\cdot h\cdot\sigma. \quad (5)$$

With h the depth of the hole, σ the surface free energy, V_m the molecular volume, and ν the number of molecules per formula unit of the dissolving phase. Similarly, as for the crystal nucleation, a hole of dissolution is only initiated if the critical size r* is reached, or in other words if $\Delta G_{diss} \leq \Delta G_{crit}$:

$$r* \approx -\frac{\sigma\cdot V_m}{\left|\Delta G_{\text{diss}}^{\frac{1}{\nu}}\right|}. \quad (6)$$

The critical size is proportional to the surface energy. Moreover, the closer the system is from equilibrium, the larger the value of r* is for the initiation of a dissolution hole.

Domain II: Domain II is placed between domains I and III and is usually difficult to characterize since it lies between two steady-state mechanisms and does not represent a steady-state itself [15]. In this part, the distance from equilibrium is superior to the critical energy barrier ($\Delta G_{diss} < \Delta G_{crit}$) to surmount for the opening of "hollow cores". For instance, screw dislocation pits will open up. A kinetic theory embodying the linear dependence with the undersaturation and the opening of crystal defects has been proposed by Lasaga et al. [14]. The model describes the bivalent role of etch pits being (1) themselves major sites of dissolution and (2) the source of dissolution steps. As it is depicted in Fig. 1, the switch between the two mechanisms can lead to a difference in the dissolution rate up to 1–2 orders of magnitude [16].

Domain I: (called dissolution plateau). The system if extremely far from equilibrium and the rate is quasi-independent of the undersaturation; it is often referred to the "distilled water" case. The scope of studies has been limited in this case to variables such as the ionic strength and the temperature. In this domain, the surface reaction is very fast and maybe faster than the molecular diffusion. In this case, the dissolved species would be depleted close to the surface, and the dissolution rate may be influenced by the transport of these species from the interface to the bulk.

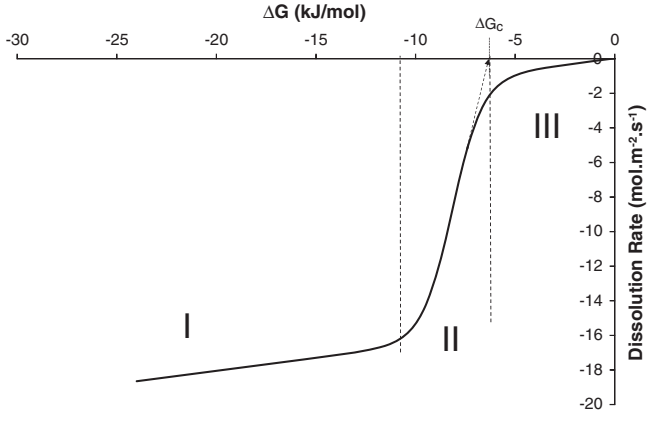

Fig. 1. Typical evolution of the dissolution rate of a mineral according to the Gibbs free energy of dissolution. Three domains can be usually recognized (see text).

The few previous studies seem to indicate that the dissolution of tricalcium silicate behaves similar to other natural silicates [17,18]. These ones are praiseworthy for shedding light on the dissolution of this phase with the usual concepts developed in geochemistry. First indications showing a strong dependence of the dissolution rate of tricalcium silicate on the undersaturation have been revealed. Moreover, as seen also in many other natural systems, the dissolution of tricalcium silicate is accompanied by the formation of etch pits, often identified by microscopy (see Fig. 2 for examples).

The present paper is mainly centered on pursuing the bridging between the dissolution kinetics and the solution chemistry as well as assessing more quantitatively the relevance of the undersaturation in dissolution kinetics of calcium silicates. From the kinetic point of view, the problem of the C–S–H precipitation is tackled in this work through the use of a specially designed reactor linked to an ICP spectrometer enabling the investigations of ultra-diluted suspensions. By doing so, the suspensions of calcium silicates are never supersaturated with respect to C–S–H during the time of experiment and the true dissolution rates are determined. From the thermodynamic point of view, the solubilities of C_3S/C_2S have never been experimentally determined but only calculated from thermodynamical data. Due to a difference of many orders of magnitude between the alite dissolution rate in pure water and in typical cement pore solutions, some recent controversial debates arose about the apparent solubilities and the calculated ones [18–20]. Provided with this new experimental set-up, it is possible to extrapolate a rate law at rate zero, i.e. when equilibrium should be matched and then to determine experimentally the standard free enthalpy of dissolution. The original discrepancy between the apparent and calculated solubilities will be discussed under the light of our experiments. Finally, we will discuss the open questions about the kinetics of early hydration of tricalcium silicate.

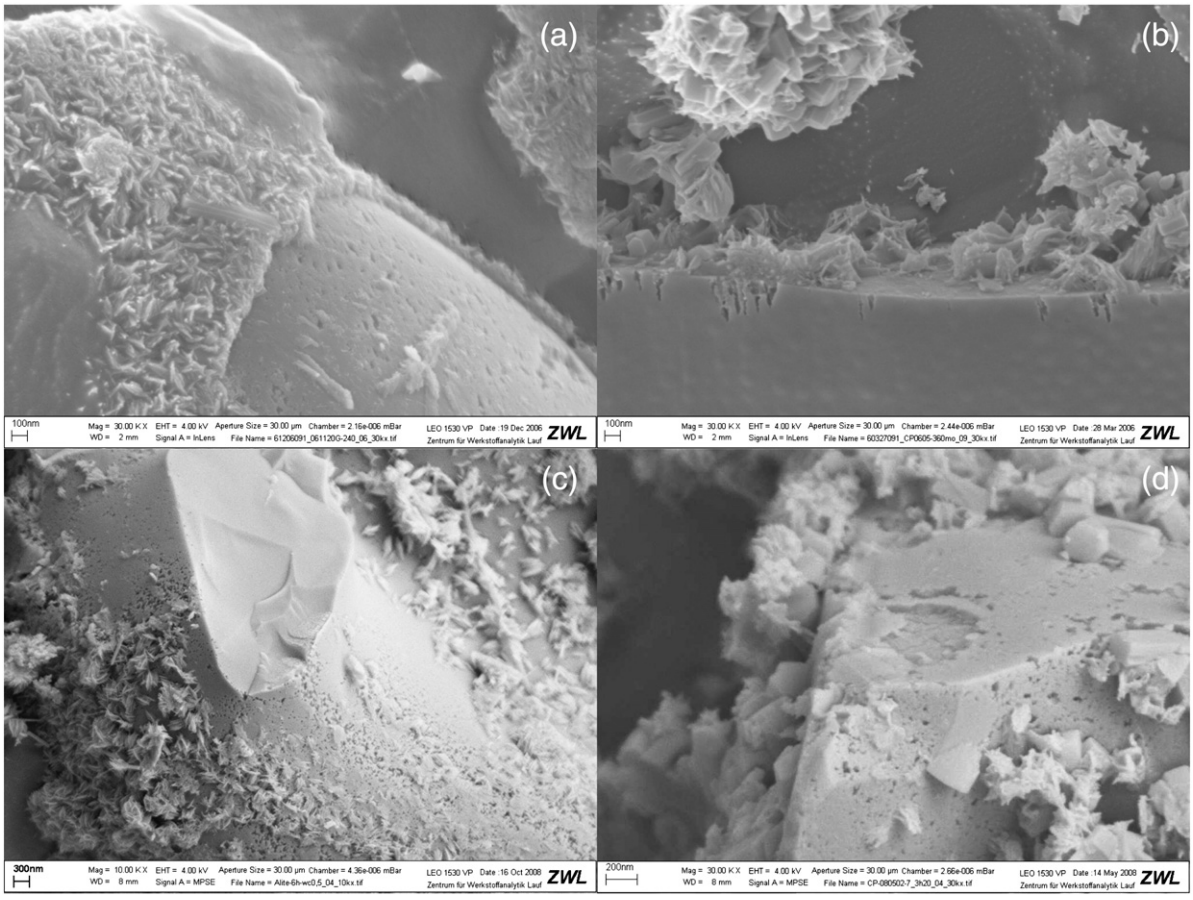

Fig. 2. Cryo-SEM pictures of various samples always hydrated at water to solid equal to 0.5 in water. (a) Cement after 4 h of hydration. The etch pits are clearly visible on the surface of this grain. They would have been probably masked if a part of the C–S–H layer had not been pulled out during the sample preparation. (b) Cement after 6 h of hydration. The depth of a couple of dissolution etch pits can be observed on this fractured grain. (c) Triclinic tricalcium silicate after 6 h of hydration. (d) Cement hydrated 200 min in presence of 0.2% of a seeding material (X-SEED®100). The grain is not much covered by the C–S–H but already strongly etched by dissolution.

As the determination of a rate law is possible over a broad range of undersaturations, we will see whether this law is sufficient to account for the dissolution of C_3S in cement, or whether it is necessary to invoke a diffusion barrier onto the C_3S grains surface [19,20]. A full rate law also valid during the cement hydration is one of last missing piece for the complete description of the C_3S or alite hydration [22].

2. Experimental part

2.1. Materials

Three different tricalcium silicates and one dicalcium silicate were studied. Two pure triclinic tricalcium silicates, referred to here as C_3S-t_1 and C_3S-t_2 respectively, and one monoclinic polymorph much closer to the tricalcium silicate phase contained in cement (alite), called C_3S-m. Both C_3S-t were obtained by solid state sintering reactions of freshly decarbonated calcium oxide and fine silica. C_3S-m was obtained by solid state sintering reactions of freshly decarbonated calcium oxide, fine silica, small quantities of alumina and MgO, followed by grinding. One sample of β-C_2S has been also used. The same synthesis procedure was used as for C_3S.

The particle size distribution was obtained by light scattering (MasterSizer 2000 from Malvern Instruments) in ethanol. Considering that the density of particles is homogeneous with the size and that the particles are spherical, we may calculate the specific surface area S_{sp} from the size distribution curve with the following formula:

$$S_{sp} = \frac{6}{\rho \cdot D_{[3,2]}}$$

where ρ is the density ($\rho_{C3S} = 3.21$ g/cm^3 and $\rho_{b\text{-}C2S} = 3.28$ g/cm^3) and $D_{[3,2]}$, the mean diameter of particles averaged over the surface of particles.

The physical characteristics of the calcium silicates are reported in Table 1 and the details of the grain size distributions in Fig. 3. The water used for the preparation of all solutions was doubly deionized.

2.2. Experimental method development

2.2.1. Experimental set-up

In order to avoid the precipitation of calcium silicate hydrate, the concentrations in the solution have to remain below the solubility limit of C–S–H which implies dissolving only a tiny quantity of anhydrous calcium silicate during the experiment time. Such a little quantity requires high precision, good time resolution and minimizing the artifacts related to sample preparation. We decided to follow the dissolution by measuring the ion concentration in solution with an ICP-OE spectrometer (Inductive Coupled Plasma — Optical Emission Spectrometer from Spectro). For this purpose, two specially designed reactors were built and connected to the spectrometer through a

Table 1
Calcium silicate polymorphs used in this study and their grain size distributions.

Sample	Polymorph	D [4,3] [um]	D [3,2] [um]	S_{sp} [m^2/g]
C_3S-t_1	Triclinic	50.16	8.53	0.22
C_3S-t_2	Triclinic	16.37	5.01	0.37
C_3S-m	Monoclinic	11.75	4.67	0.40
β-C_2S	Monoclinic	23.43	0.62	2.93

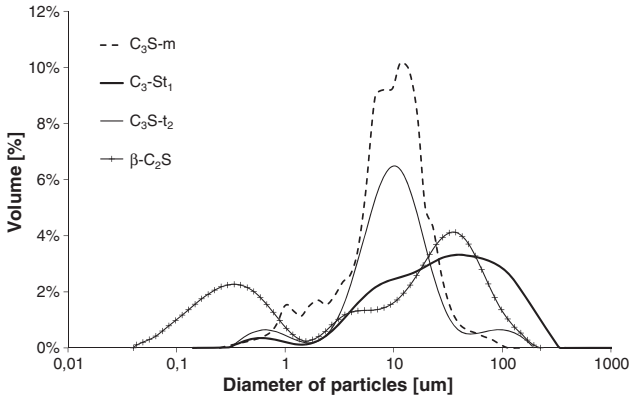

Fig. 3. Grain size distributions of the various anhydrous calcium silicates used in this study.

filtering device. They only differ by the filtering and injection systems. One of them is schematically depicted in Fig. 4. The reactor with a capacity of 1 L is directly connected to the ICP. The solution from the reactor is sucked up via a peristaltic pump, goes through a first filter and is then pressed through a second filter with a porosity of 0.1 μm. Most of the solution flows back into the reactor. A capillary tube usually connected to the spectrometer sample holder, is grafted onto the output tube and allows for the rapid transfer of a little part of the freshly filtered solution to the ICP nebulizer. Only about 1% of the solution is really nebulized and heated in the plasma, the rest is collected and usually evacuated. We also bypassed this tube in order to re-inject the non-consumed solution into the reactor. Using this principle, only 9 mL of solution per hour is consumed. Taking into account the original volume of 1 L, the concentration factor of solid over time is small. The volume of solution in all tubes is about 8 mL which is negligible compared to the volume dwelling in the reactor. We therefore consider that there is only a delay between the measurement and the dissolution due to the time for the solution to reach the torch but no inertia at all. A flow of nitrogen gas is ensured in the reactor in order to prevent the carbonation reactions. The spectrometer and a rapid integration of the spectrum allow for 3–4 analyses per minute.

2.2.2. Experimental conditions

As mentioned above, the pure dissolution of anhydrous calcium silicates is carefully studied as far as the solution is not supersaturated with respect to C–S–H. We calculated the maximum quantity of C_3S or C_2S which can be mixed with water, i.e., the minimum initial liquid to solid ratio, without reaching the solubility limit of C–S–H even if the entire calcium silicate is dissolved. The latter strongly depends on the concentration of calcium hydroxide [23]. The minimum liquid to solid ratios according to different concentrations in lime are reported in Table 2. Instead of fixing a high liquid to solid ratio, we may also start with a lower one and look at the maximum of C_3S which may be dissolved in undersaturation with respect to C–S–H. We do not repeat the calculations for the C_2S since 1 g of C_2S totally dissolved will lead to a lower supersaturation with respect to the C–S–H than 1 g of C_3S.

2.2.3. Method validation

Fig. 5 shows the evolution of Ca and Si concentrations during the dissolution of C_3S and C_2S in doubly de-ionized water. The concentration of calcium is exactly 3 times and 2 times, respectively, higher than the silica concentration, i.e. the dissolution of C_3S and C_2S is congruent as originally proposed by Le Chatelier and generally accepted today. The concentrations increase rapidly at the beginning and finally approach a constant value corresponding to the complete dissolution of the anhydrous calcium silicate considered. Exactly the same results were obtained with both experimental devices. Batch experiments were also performed in the same stirring conditions; they are also in agreement with the values obtained by continuous measurements. All results are reported in Fig. 5.

2.2.4. Determination of the interfacial dissolution rate

During the set of experiments, we varied the initial concentration of calcium hydroxide among other parameters, making it impossible to accurately follow the Ca concentration (except in water). The dissolution is therefore only monitored by the concentration of Si, which allows for the determination of the dissolution rate since the stoichiometry is maintained during the dissolution. The estimation of the interfacial dissolution rate requires a low uncertainty with respect to the surface area of C_3S or C_2S in contact with water. It is not a trivial problem to calculate the latter since the grain size is decreasing during the dissolution experiment resulting in grain size distribution narrowing. Moreover, the dissolution may occur by the formation and opening of etch pits which are likely to increase the real contact surface with water [24]. For the sake of pragmatism and to minimize uncertainty, we approximated the dissolution rate by the slope of the curve $Si = f(t)$ calculated on the 3 or 4 first points i.e. during the first 40 s of dissolution. In this range, the volume of calcium silicate dissolved is small and we may neglect the

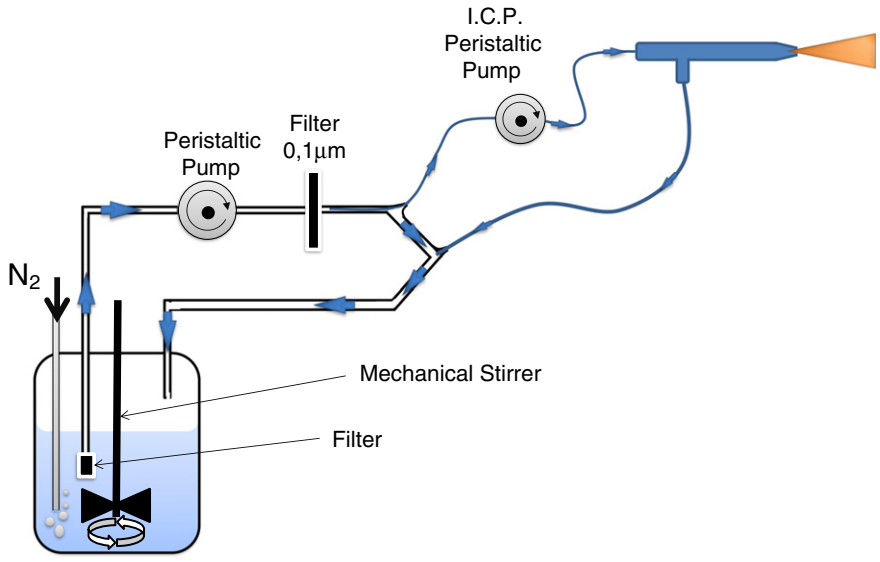

Fig. 4. Sketch of one of the experimental set-ups built for monitoring ion concentrations during the dissolution of minerals in diluted suspensions.

Table 2
Estimations of the maximum amounts of C_3S or C_2S which can be initially used or the maximum of C_3S/C_2S which can be dissolved in order to remain undersaturated with respect to C–S–H in all dissolution experiments. The equilibriums used for the calculus of the C–S–H solubilities are listed in Table 10.

$[Ca(OH)_2]$ initial	Conditions for no C–S–H precipitation during exp.	
[mM]	L/S_{min} if 100% C_3S or C_2S dissolved	L/S = 10,000, %max C_3S or C_2S to dissolve
		[%]
0	10,000	100
5	25,000	40
10	45,000	22
15	60,000	17
20	80,000	13

variation of the surface area as a first approximation. The surface area is then considered constant and equal to the initial specific area.

3. Thermodynamic framework

Considering any reversible reaction, for instance the dissolution in Eq. (1), the change in free enthalpy corresponding to this reaction at temperature and constant pressure is given by the Eq. (2).

In the case of a hydrolysis, the mineral A_xB_y reacts with water. At the equilibrium, the change in free enthalpy is zero which yields:

$$\Delta_{diss}G^0 = -RT\ln K \text{ and } K = (A)^x_{eq.}(B)^y_{eq.} \quad (7)$$

with $(A)_{eq.}$ and $(B)_{eq.}$ the activities of A and B in solution at the equilibrium. For dissolution or precipitation reactions, K is defined as the solubility product $K = K_{sp}$. The ion activity product Π corresponding to the above chemical equation is in this case:

$$\Pi = (A)^x(B)^y \quad (8)$$

for $\Pi < K_{sp}$, the solution is undersaturated; for $\Pi > K_{sp}$, the solution is supersaturated. The undersaturation and supersaturation are both deviations from equilibrium and the driving forces for the dissolution and crystal growth, respectively. The determination of the solubility is a way to determine $\Delta_{diss}G°$. Latter can be also calculated with any other reaction path starting with xA + yB and leading to A_xB_y at the end, as for instance:

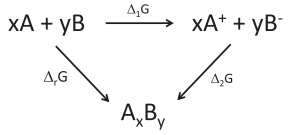

We may then write a Bordwell thermodynamic cycle enabling us to calculate $\Delta_rG°$, if $\Delta_1G°$ and $\Delta_2G°$ are known, with the simple relation $\Delta_rG° = \Delta_1G° + \Delta_2G°$.

The ion activities are calculated with the speciation software Phreeqc v2.13. The relevant database for the speciation is shown in Table 10. In said version of Phreeqc, the activity coefficients are calculated with the extended Debye–Hückel equation which obviously remains an approximation. Nevertheless, we may use it with a sufficient degree of confidence since the ion concentrations are rather low and no divalent ions are present other than the calcium ions. The concentration of OH^- is obtained from the charge balance.

The estimation of the solubility product of C_3S (or C_2S) done by many authors [20,25,26] is based on the calculation of the free enthalpy involved in the following hydrolysis reactions. We also introduce the reaction of quicklime (CaO) with water as it will be needed later on.

$$Ca_3SiO_5 \xrightarrow{\Delta_{hydrolysis}G^0(C_3S)} 3Ca^{2+} + H_4SiO_4 + 6OH^- \quad (9)$$

$$Ca_2SiO_4 \xrightarrow{\Delta_{hydrolysis}G^0(C_2S)} 2Ca^{2+} + H_4SiO_4 + 4OH^- \quad (10)$$

$$CaO \xrightarrow{\Delta_{hydrolysis}G^0(C)} Ca^{2+} + 2OH^-. \quad (11)$$

We expressed the hydrolyses with the species H_4SiO_4 as part of the products whereas it is not the most stable silicate species at high pH, keeping in mind that the following equilibriums exist simultaneously:

$$H_4SiO_4 + OH^- \leftrightarrows H_3SiO_4^- + H_2O \quad (12)$$

$$H_3SiO_4^- + OH^- \leftrightarrows H_2SiO_4^{2-} + H_2O. \quad (13)$$

Additionally, the total molar concentration of Si is low and oligomerization can therefore be neglected. As was said, energies involved in the hydrolysis reactions are not known but can be determined from the Gibbs energies of formation, it yields:

$$\Delta_rG°(C_3S) = 3\Delta_fG°\left(Ca^{2+}_{(aq)}\right) + 6\Delta_fG°\left(OH^-_{(aq)}\right) + \Delta_fG°\left(H_4SiO_{4(aq)}\right) - \Delta_fG°(C_3S) - 5\Delta_fG°(H_2O_{(l)}{}^2)$$

$$\Delta_rG°(C_2S) = 2\Delta_fG°\left(Ca^{2+}_{(aq)}\right) + 4\Delta_fG°\left(OH^-_{(aq)}\right) + \Delta_fG°\left(H_4SiO_{4(aq)}\right) - \Delta_fG°(C_2S) - 4\Delta_fG°(H_2O_{(l)}{}^2)$$

$$\Delta_rG°(C) = \Delta_fG°\left(Ca^{2+}_{(aq)}\right) + 2\Delta_fG°\left(OH^-_{(aq)}\right) - \Delta_fG°(C) - \Delta_fG°\left(H_2O_{(l)}{}^2\right).$$

Very discrepant values arise from the literature which motivated us to repeat the calculus (see Table 3). For this, the changes in enthalpies of formation have to be determined, the standard Gibbs enthalpy for a reaction of formation at 298 K is:

$$\Delta_fG°_{298\ K} = \Delta_fH°_{298\ K} - T\cdot\Delta_fS°_{298\ K}. \quad (14)$$

Even if the changes in free enthalpy of many species are known nowadays, some still require to be calculated?, i.e., the heat of formation $\Delta_fH°$ and the variation in entropy $\Delta_fS°$ have to be determined. We found all the values for the heat of formation in reliable databanks

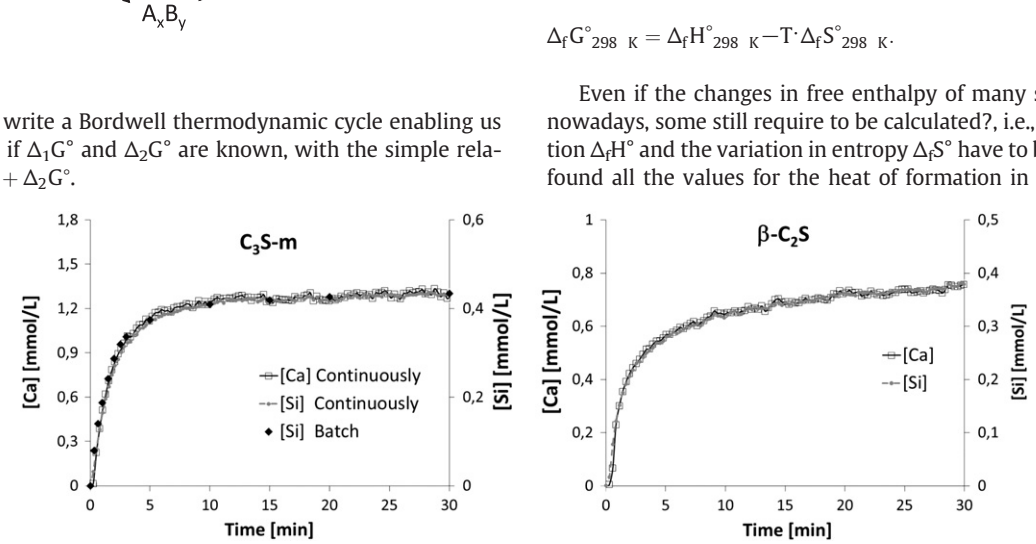

Fig. 5. Evolution of Ca and Si concentrations during the dissolution of C_3S and C_2S in distilled water. Liquid to solid ratio = 10,000, stirring rate = 500 rpm, T = 25 °C. The double Y-axes are scaled in order to match the congruency. The curves [Ca] = f(t) and [Si] = f(t) are then superimposed.

Table 3
Thermodynamic database used for (a) the calculation of the free enthalpies of formation $\Delta_f G°$ and (b) the change in free enthalpies $\Delta_r G°$ during the hydrolysis of C_3S, C_2S and CaO referring to Eqs. (9)–(11).

Species in reference state	S° 1bar	$\Delta_f H°$	$\Delta_f S°$	$\Delta_f G°$	$\Delta_r G°$
	J/mol/K	kJ/mol	J/mol/K	kJ/mol	kJ/mol
Si(s)	18.81[a]				
Ca(s) beta phase	41.59[a]				
O_2(g)	205.15[a]				
H_2(g)	130.68[a]				
H_2O(l)	69.95[a]	−285.5[a]	−163.3	−236.9	
OH^-(aq)	−10.9[b]	−230.0[b]	−244.3	−157.2	
H_4SiO_4(aq)	180.87[c]	−1460.91[c]	−509.0	−1309.23	
Ca^{2+}(aq)	−53.1[b]	−542.8[b]	36.2[b]	−553.6	
Ca_3SiO_5	169.0[d]	−2931.0[d]	−487.5	**−2785.7**	**56.8**
Ca_2SiO_4	128.0[d]	−2308.0[d]	−384.3	**−2193.5**	**95.7**
CaO	38.1[b]	−634.9[b]	−106.1	**−603.3**	**−27.8**
$C_3S-(C_2S+CaO)$		11.9		11.0	

[a] M.W. Chase [27].
[b] Handbook of Chemistry and Physics [28].
[c] J.D. Rimstidt [29].
[d] V.J. Babushkin [30]).

(see Table 3). The variation in entropy is calculated from the absolute entropies $S°_{i,298}$:

$$\Delta_f S°_{298\ K} = \sum_i \upsilon_i \cdot S°_{i,298} \quad (15)$$

with υ_i the stoichiometric coefficient of the species i. In Table 3 the thermodynamical values used for the calculus of free enthalpies of formation and the change in free enthalpies during the hydrolysis of C_3S, C_2S and CaO are listed.

It is interesting to calculate the energetic difference between C_3S and C_2S+CaO since it should correspond to the energy involved in the reaction $C_2S+CaO \rightarrow C_3S$ during the clinkerization. The usual accepted value is around 10 kJ/mol [1] which is close to our value. In Table 4, we listed the enthalpy changes during the hydrolysis of C_3S and C_2S obtained from literature data and from this study. As values depend on the reference hydrolysis reaction, i.e. the silicate species involved, these ones are indicated. Most of these values are in the same range: they are positive and therefore characteristic of equilibrated reactions. The main source of discrepancy on final $\Delta_d G°$, is the standard free enthalpy of formation of the silicate species. We chose $H_4SiO_{4(aq)}$ and a value calculated from recent determinations of quartz solubility at low temperatures [29] and of amorphous silica solubility [31]:

$$SiO_{2(s)} + 2H_2O \rightarrow H_4SiO_{4(aq)}. \quad (16)$$

This solubility equilibrium has been characterized with careful attention and the true solubility limit of silica has been measured. We have to put a bit more caution on the formation enthalpies of deprotonated species.

As it has been historically for the first time concluded by Stein [25] the change in free enthalpy of the C_3S/C_2S hydrolyses calculated from the enthalpies of formation is high. It is not possible to directly compare the free enthalpies because they do not correspond to reactions involving the same species. In return, we may calculate the solubility products according to the equations involved in the respective articles as well as the solubility. Such a range of values correspond to a relatively high solubility incompatible with some experimental evidences. It is clear, by only looking at the spread of values in Table 4, that the calculus using the enthalpies of formation is faulty. It is a known problem [33] arising when the species in equilibrium are not perfectly known and characterized. This fact motivated us to determine the solubility by other means, as here from a kinetic approach.

4. Experimental results

4.1. Role of the diffusion layer on the dissolution rate

The dissolution rate is controlled by the local concentrations at the grain–water interface but the concentrations are measured in the bulk. An accumulation of ions at the interface occurs when the ions released by the dissolution are not transported rapidly enough into the bulk. Then the deviation from equilibrium at the interface will be significantly lower than in the bulk and the overall dissolution rate will be reduced. The transport of ions depends on the diffusion coefficients of these ions, advection and convection. The relative influence of the diffusion on the overall dissolution rate has to be considered only if the interfacial dissolution rate of any ion is of the same order of magnitude as its diffusion rate. It has been checked here by varying the stirring rate when the dissolution is fast i.e. in the case of distilled water (see Fig. 6). A decrease in the overall rate is observed at 330 rpm. As a consequence the stirring rate does not play a major role at least in a range above 500 rpm when the dissolution starts in distilled water. In the following we fixed the stirring rate at 500 rpm for all experiments. The dissolution of C_2S is slower than C_3S, the diffusion does not play a major role too.

4.2. C_3S/C_2S dissolution in distilled water

The continuous measurement of the silica concentration during the dissolution of C_3S in water at W/C = 10,000 and 50,000 is illustrated in Fig. 7. The initial rate is high and does not depend on the W/C ratio during most of the dissolution. It means that, under these conditions, the distance from equilibrium is high enough for the interfacial rate to be independent of the undersaturation. This is not the case for C_2S. Indeed, the dissolution at L/S = 10,000 runs significantly slower than at L/S = 50,000 (Fig. 7). This means that the solution approaches the solubility equilibrium during the dissolution at L/S = 10,000 enough in order to influence the dissolution rate and thus reduce it according to the deviation.

4.3. C_3S and C_2S dissolutions in lime solutions

It is well known that the calcium hydroxide concentration is a key parameter controlling the hydration of both anhydrous silicate phases. When C_3S or C_2S dissolves in lime solutions instead of pure water, the dissolution rate strongly decreases as the initial lime concentration increases (Fig. 8), as it has been already reported [17–35] for C_3S. It thus means that the higher the concentration in calcium hydroxide in cement, the lower the dissolution of alite or belite. All factors which might decrease or limit the calcium and hydroxide concentration in cement, as the precipitation of Portlandite, will favor the dissolution

Table 4
Values of $\Delta_r G°$ for the hydrolysis of C_3S and C_2S from the literature and calculated in this study. S_c are the solubilities calculated from the free enthalpies.

References C_3S	Silicate considered	$\Delta_r G°$ C_3S [kJ/mol]	s_c [g/L]	References C_2S	Silicate considered	$\Delta rG°$ C_2S [kJ/mol]	s_c [g/L]
Stein [25]	H_4SiO_4	13.86	32.0	Data from Babushkin [30]	$H_2SiO_4^{2-}$	61.51	0.04
Barret [32]	H_3SiO4^-	33.18	14.6	This study	H_4SiO_4	95.7	0.26
Bellmann [20]	$H_2SiO_4^{2-}$	22.5	24.3				
This study	H_4SiO_4	56.8	5.7				

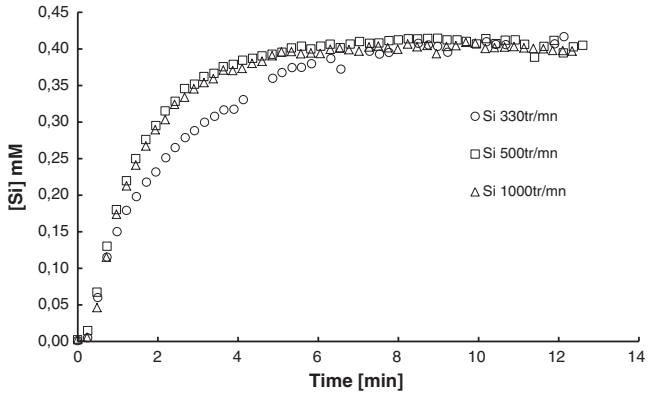

Fig. 6. The Si concentration in solution over time during the dissolution of C_3S in water at various different stirring rates. W/C = 10,000, T° = 25 °C.

of alite or belite. The decrease of the dissolution rate with the calcium hydroxide concentration is more pronounced for C_2S.

4.4. Experiments data set

We systematically measured the rate of dissolution of C_3S, C_2S and CaO in different solutions characterized by various deviations from equilibrium varying calcium, silicate, hydroxide concentrations and ionic strength. All the dissolution experiments in ultra-diluted conditions are reported in Table 11. Most of the experiments have been duplicated or triplicated. The concentrations measured by ICP spectrometry are also averaged over the first 3–4 points and we calculated a mean ion activity product related to these points with Phreeqc.

5. Discussion

5.1. Dissolution kinetics and determination of the experimental solubility products of Ca_3SiO_5, Ca_2SiO_4 and CaO

The ion activity products and the changes in free enthalpy changes corresponding to the dissolution of C_3S, C_2S and CaO (Eqs. (9)–(11)) are:

$$\Pi_{C_3S} = \left(Ca^{2+}\right)^3 (H_4SiO_4)(OH^-)^6 \tag{17}$$

$$\Pi_{C_2S} = \left(Ca^{2+}\right)^2 (H_4SiO_4)(OH^-)^4 \tag{18}$$

$$\Pi_{CaO} = \left(Ca^{2+}\right)(OH^-)^2 \tag{19}$$

$$\Delta_{diss}G_{C_3S,C_2S,C} = \Delta_{diss}G^\circ{}_{C_3S,C_2S,C} + RT\ln\Pi_{C_3S,C_2S,C}. \tag{20}$$

As outlined in the introduction, dissolution kinetics of minerals depends on the variation of the dissolution free enthalpy, i.e. the deviation from solubility equilibrium. As discussed above, ΔG° being only estimated, we chose to plot the dissolution rate, not as a function of the free enthalpy, but rather as a function of $\ln \Pi$. This plot directly gives the actual solubility product by extrapolation at dissolution rate null, i.e., when the system reaches equilibrium. These plots are presented in Figs. 9–11 for C_3S, C_2S and CaO, respectively.

5.1.1. The tricalcium silicate

Looking at Fig. 9, we see that all kinetic curves $R = f(\ln \Pi)$ tend to the same point at dissolution rate zero, being the experimental solubility product. The three typical kinetic domains can easily be identified with the triclinic C_3S polymorphs. They cannot be clearly distinguished from the monoclinic C_3S, highlighting different dissolution behaviors far from equilibrium probably due to different crystal energies and/or defects densities. All the curves can be fitted over the entire range of deviation from equilibrium using a simple algorithm dividing the procedure into two parts. The first part focusing on the low $\ln \Pi$s is fitted with a first Boltzmann function y_1 and the second part with another Boltzmann function y_2 for the high $\ln \Pi$s:

$$y_1 = \frac{A_1 - B_1}{1 + \exp\left(\frac{\ln\Pi - x_{0_1}}{d_1}\right)} + B_1; \quad y_2 = \frac{A_2 - B_2}{1 + \exp\left(\frac{\ln\Pi - x_{0_2}}{d_2}\right)} + B_2. \tag{21}$$

The interfacial dissolution rate is then given by:

$$R = y_1 \quad \text{if} \quad \ln\Pi < \ln\Pi_b \quad \text{and} \quad R = y_2 \quad \text{if} \quad \ln\Pi \geq \ln\Pi_b \tag{22}$$

where the interfacial rate R is expressed in $\mu mol/m^2/s$. $\ln \Pi_b$ corresponds to the limit for switching from the first Boltzmann function to the second one. As an example, the C_3S-t_1 curve (Fig. 9) is fitted with the set of parameters found in Table 5.

The fitting function does not have any physical meaning but only gives a useful mathematical representation of the kinetics of dissolution. The intercept with the X-axis gives $\ln \Pi = -50.7 \pm 0.5$ corresponding to $K_{sp} = 9.6 \cdot 10^{-23}$ and $\Delta G^\circ = 125.7 \pm 1$ kJ·mol^{-1}. We remind that no calcium silicate hydrate is likely to precipitate in these experiments.

The important point differentiating the dissolution of C_3S-t and C_3S-m is that the experiments done on both triclinic C_3S undoubtedly show the switch between the two dissolution mechanisms. Within the experiment series carried out with C_3S-t, the critical energy for the opening of etch pits was low enough to be rapidly reached within the range of the experimental undersaturations. We may estimate the excess of undersaturation ($\ln \Pi_{crit.} - \ln K_{sp}$) corresponding to the energy for opening the etch pits. This energy is estimated at about ~31 kJ/mol for the C_3S-t_1 and ~40 kJ/mol for the C_3S-t_2. This energy corresponds to the congruent dissolution of approximately 1 mM of C_3S. Independent of the C_3S used, such low concentrations are achieved quasi instantaneously in paste, meaning that such a deviation from equilibrium can be encountered only shortly and never maintained in concentrated

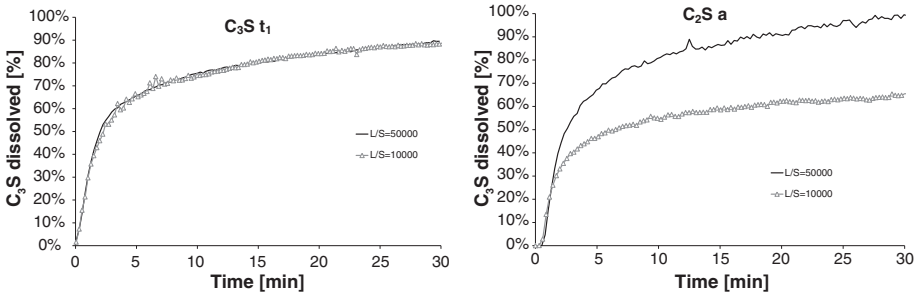

Fig. 7. Evolution of the percentage of C_3S-t_1 or C_2S dissolved over time in water at two different liquid to solid ratios (L/S).

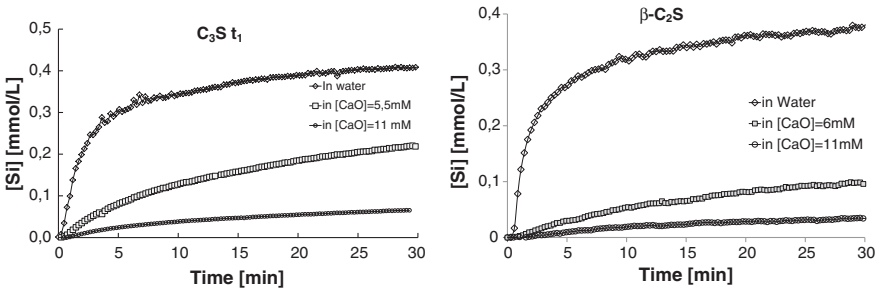

Fig. 8. Tricalcium silicate and dicalcium silicate dissolutions in different initial lime solutions at W/C = 10,000 and stirring rate at 500 rpm over time.

systems. As the dissolution curves are nearly merged approaching the equilibrium, meaning that the three C_3S dissolves likewise approaching the solubility, we may consider that the reported law for the C_3S-t_1 can be used with confidence for any C_3S to calculate its dissolution rate from the ion concentrations in solution, without repeating the same study as in this paper. The domain of validity for any C_3S, according to our study, is reasonable for $\ln \Pi > -62$.

5.1.2. The dicalcium silicate

The same kind of experiments was repeated with dicalcium silicate. In Fig. 10, the dissolution rate of β-C_2S has been observed according to the logarithm of the ion activity product as defined in Eq. (18). The three kinetic domains may be assigned. The curve is fitted with the abovementioned procedure and the set of parameters given in Table 6.

The curve intercepts the X-axis at $\ln \Pi = -40 \pm 0.8$, which then gives $K_{sp} = 4.3 \cdot 10^{-18}$ and $\Delta G^\circ = 99.2 \pm 2$ kJ/mol. The energy corresponding to the opening of defects is then equal to about 31 kJ/mol considering the deviation from the equilibrium.

5.1.3. The quicklime, CaO

Since the experimental determination of the solubility of quicklime is essential in the further thermodynamical calculations we will develop, we also apply the same strategy for CaO. CaO was obtained by decarbonation of pure $CaCO_3$ at 900 °C overnight and used immediately after its cooling. The number of experiments forced us to repeat the decarbonation many times. Therefore, we did not work exactly with the same material for all experiments which inevitably leads to some variations of the specific surface area. As the determination of the surface area is difficult for such a reactive material, we expressed the dissolution rate by g of product and not by m^2 as previously. Basically three sets of experiments were done. The first one consists of dissolutions of 0.1 g/L CaO in lime solutions, the second one consists of dissolutions of 0.1 g/L CaO in NaOH solutions and the third one in KOH solutions. During all experiments, the solutions always remained undersaturated with respect to Portlandite $Ca(OH)_2$. The dissolution rates as a function of ln Π, defined in Eq. (19), are represented in Fig. 11. Whereas the behaviors in NaOH/KOH and CaO solutions are different, we clearly see that the three curves tend towards $\ln \Pi = -11.7 \pm 0.5$ at rate = 0. As it will be explained below, this difference between the dissolution rate in CaO and NaOH solutions may be reasonably attributed to electrostatic phenomena at the interface. We observe that for the same undersaturation, the dissolution rate in NaOH/KOH solutions is lower than that in $Ca(OH)_2$ solutions. In NaOH/KOH solutions, the pH is higher leading to a more negative surface charge possibly further limiting the dissolution rate.

These results are similar to what could be estimated from another experimental data set [36]. Indeed, Ritchie also determined the dissolution rate of CaO, in NaOH solutions under conditions where Portlandite did not precipitate, with the known rotating disk method. In this article, at very high rotation speed, the overall dissolution rate is determined by the reaction rate. From Fig. 10 of Ritchies's article, it can be estimated that the dissolution rate of CaO approaches zero when the ion activity product in the solution tends towards the solubility product of Portlandite, even if Portlandite does not precipitate.

With our kinetic approach, we found that the value of ln Π at rate = 0 is close to the logarithm of the solubility product of $Ca(OH)_2$ (−11.7). In order to differentiate both and to more carefully determine the solubility product of CaO, additional experiments were performed with more material. In those ones, the solution was not always under undersaturated conditions. In Fig. 12, we see that a metastable plateau is

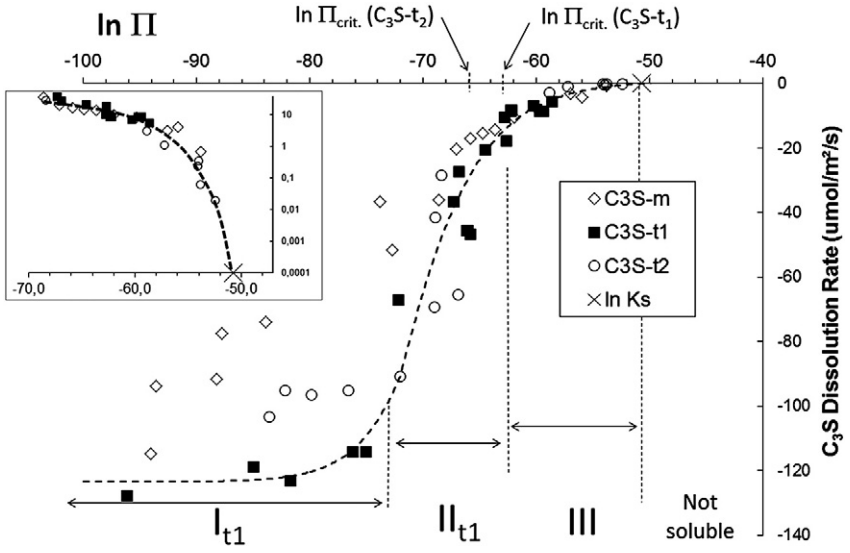

Fig. 9. The dissolution rate of the three C_3S samples as a function of ln Π. The boundaries between the kinetic domains and the typical S-curve resulting from the algorithm realized by Eqs. (21) and (22) are represented only for C_3S-t_1. A logarithm plot (with a reversed sign for the rate) is also shown in inset for the determination of the solubility product.

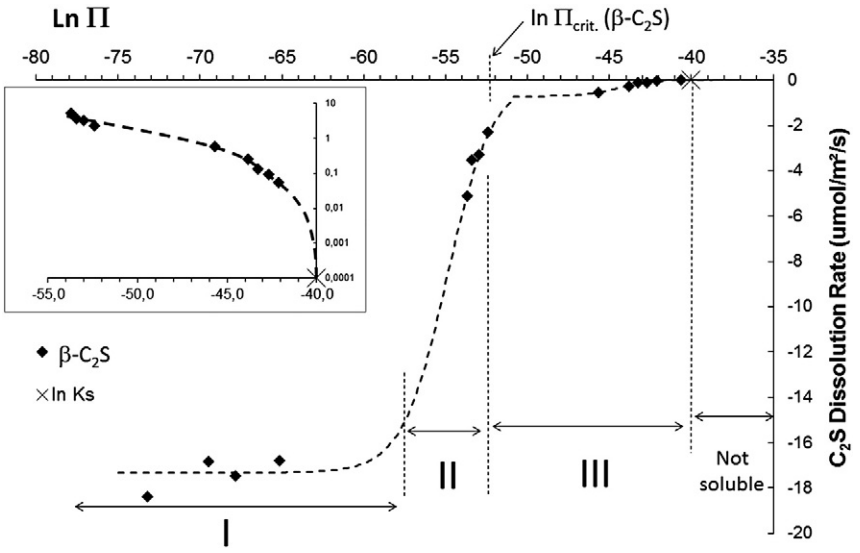

Fig. 10. The dissolution rate of C_2S as a function of ln Π. The dashed curve represents the fit done with the set of parameters shown in Table 6. A logarithm plot (reversed sign) is also proposed in inset for the determination of the solubility product.

reached when 0.5 g/L of CaO is dissolved in a solution of 22 mmol/L of $Ca(OH)_2$ or when 2 g/L of CaO is dissolved in water. In both, there are still CaO particles in the reactor at the end of the experiment. This plateau in [Ca] is a bit higher than the solubility of $Ca(OH)_2$ and corresponds to a value of ln Π = −11.62. Both determinations of the solubility at 20 °C, under metastable or undersaturated conditions, tend to the same value. It indicates that the determination in metastable conditions really corresponds to the true solubility of CaO. Thus, we obtain for CaO, $[Ca]_{eq}$ = 25.20 mmol/L. We found for $Ca(OH)_2$, $[Ca]_{eq}$ = 24.45 mmol/L. As it will be demonstrated below, equilibrium reactions occur at the interface and therefore depend on the surface which is in contact with water. In this respect, there is no reason as to why the $Ca(OH)_2$–water and the CaO–water interfaces differ a lot, meaning that their solubilities should be close.

5.2. Origin of the discrepancy within the solubility products

We reported in Table 7 the differences between the values of the free enthalpy of dissolution we deduced from the dissolution rates with the values calculated above from the free enthalpies of formation (see Table 3). The difference is huge in case of C_3S and CaO, and limited in case of C_2S.

The minerals we investigated all have unsaturated oxygen atoms present on their surfaces, which in water will be protonated to a varying degree according to the pH of the solution and the electronegativity of the respective oxygen atoms. At the interface, the following reactions with water and protons are relevant:

$$> O^{2-} + nH_2O \rightarrow > OH_n^{n-2} + nOH^- \quad 1 \le n \le 2$$
$$> SiO_4^{4-} + nH_2O \rightarrow > H_nSiO_4^{n-4} + nOH^- \quad 1 \le n \le 4$$
$$> O^{2-} + nH^+ \rightarrow > OH_n^{n-2} \quad 1 \le n \le 2$$
$$> SiO_4^{4-} + nH^+ \rightarrow > H_nSiO_4^{n-4} \quad 1 \le n \le 4.$$

These reactions of protonation occur extremely rapidly and change the mineral/water interface and the interfacial crystal energy. It is also possible to argue further that water molecules play a role in the stabilization of silicate surfaces as it has been highlighted by Lasaga et al. using ab initio modeling [37]. The species formed are in equilibrium with the tricalcium/dicalcium silicate solutes. This will lead to a variation of the surface charge which changes the properties of the interface and

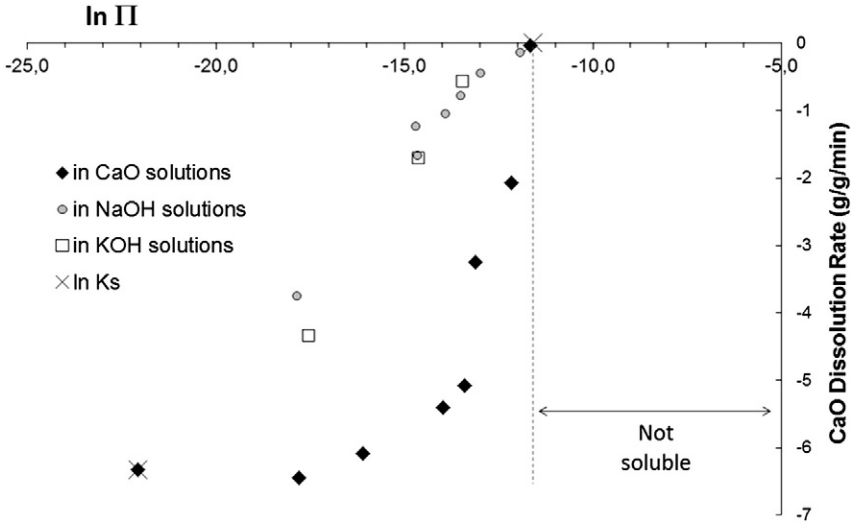

Fig. 11. The dissolution rate of CaO as a function of ln Π.

Table 5
Set of fit parameters for C_3S-t_1.

A_1	−123.44	A_2	−264.19	ln Π_b	−72
B_1	2.14	B_2	0.92		
$X0_1$	−68.88	$X0_2$	−74.72		
d_1	2.99	d_2	4.26		

therefore of the mineral. Two of these properties are the solubility of the mineral and the dependence of the dissolution rate on pH. In general terms, it is well recognized that apparent surface equilibrium constants are a function of surface charge or potential, comprehensive papers review the related issues [38–41]. Focusing on a simple mineral such as silica among various data available, it was demonstrated that the dissolution rate of quartz can be very well modeled over a broad range of pH and temperature taking into account the different protonations of the surface silica tetrahedra [42] or in terms of surface potential [43].

In addition, it is obvious that the respective dissolutions of C_3S, C_2S and CaO are irreversible and will never be formed in aqueous medium. As a matter of fact, calcium silicates and calcium oxide are iono-covalent crystals constituted by Ca^{2+}, O^{2-} and SiO_4^{4-}–Ca^{2+}, SiO_4^{4-} and Ca^{2+}, O^{2-}, respectively. The species O^{2-} and SiO_4^{4-} do not exist in aqueous solutions. The stable species are the hydroxylated species OH^- and $H_3SiO_4^-/H_2SiO_4^{2-}$ respectively for the pH encountered during C_3S dissolution in water. O^{2-} and SiO_4^{4-} cannot be formed at room temperature from the hydroxylated species, hence the impossibility to write a simple solubility equilibrium for C_3S, C_2S and CaO with their constituents O^{2-} and SiO_4^{4-}. It is necessary to consider first the superficial protonation leading to the hydroxylated species [32]. Experimentally, we determined the solubility equilibriums between the solute and these hydroxylated surfaces according to

$$C_3S_{\text{hydroxylated surface}} \leftrightarrows 3Ca^{2+} + H_4SiO_4 + 6OH^- \quad (23)$$

$$C_2S_{\text{hydroxylated surface}} \leftrightarrows 2Ca^{2+} + H_4SiO_4 + 4OH^- \quad (24)$$

$$CaO_{\text{hydroxylated surface}} \leftrightarrows Ca^{2+} + 2OH^- \quad (25)$$

when the free enthalpies of dissolution reported in Table 3 correspond to the fully deprotonated surface, i.e., to pH not encountered in aqueous solutions.

The influence of the surface charge, varying with pH, on the free enthalpy of dissolution can be shown in the case of C_2S. Solutions saturated with respect to C_2S and consequently metastable with respect to C–S–H, i.e. not supersaturated enough to immediately precipitate C–S–H, have been reported [44,45]. Referring to the data published in these papers, one sees that the values of [Ca] and [SiO_2] corresponding to saturated solutions of C_2S lie between two curves, calculated using two solubility products, corresponding to $\Delta G_1 = 103.4$ and $\Delta G_2 = 100.6$ kJ/mol. The variation of the free energy of dissolution is therefore about 2.8 kJ/mol. This variation, due to the difference of surface charge on C_2S, is linear at least between pH = 12.26 and 12.56 (Fig. 13).

The standard free enthalpy can be written as a sum of an ideal term corresponding to a neutral surface charge plus an excess of free enthalpy due to the surface charge. The latter is depending on pH. Unfortunately, it is not possible to determine the ideal term of the free enthalpy since the point of zero charge is not known for C_2S. However, from the calculated $\Delta G°$ value (95.7 kJ/mol) which would correspond to a fully deprotonated surface, we can estimate the pH necessary for this full deprotonation. Indeed, assuming a linear law between the pH and $\Delta G°$ (reported in Fig. 13), one finds about pH = 13.26 which is a reasonable value for silicates. The solubility product ($\Delta G° = 99.2$ kJ/mol) estimated with our kinetic approach, corresponds to a degree of deprotonation only reached at high pH if we refer to the curve in Fig. 13, which is the right trend. Nevertheless, it is important to keep in mind that the solubility value of C_3S will also vary with pH, i.e., our estimated solubility is given for a certain pH and it should be a bit more soluble at even higher pH.

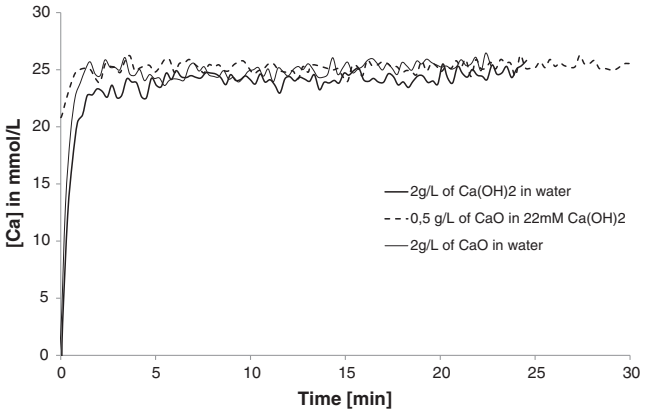

Fig. 12. Concentration of Ca in solution during the dissolutions at 20 °C of $Ca(OH)_2$ and freshly burned CaO. The plateaus in Ca correspond to their respective solubilities. CaO is about 0.7 mM more soluble than $Ca(OH)_2$.

In order to check the validity of our hypothesis assuming that differences in energy between the calculated solubilities and experimental ones are due to the protonation of silicate and oxide ions at the surface of minerals, we examined whether deviations observed in C_3S, C_2S and CaO are together consistent. Indeed, tricalcium silicate consists of monomeric silicate tetrahedra SiO_4^{4-}, calcium ions Ca^{2+} and oxygen ions O^{2-}. Dicalcium silicate only contains monomeric silicates and the quick lime only oxide ions. The crystal structures are depicted in Fig. 14. In addition, taking into account the respective molar volumes (reported in Table 7) one finds that the added molar volumes of CaO and C_2S are similar to the molar volume of C_3S; as a simplification we may then consider $C_3S = C_2S + CaO$.

The deviation $\Delta_rG° - \Delta_dG°$ is 68.9 kJ/mol for C_3S corresponds to the surface charge effect at the interface C_3S/water. The sum of deviations observed with C_2S and CaO is equal to 60.1 kJ/mol, very close to the deviation observed with C_3S. The difference $\Delta C_3S - (C_2S + CaO))$ is only 8.7 kJ/mol. This difference means that it is probably a bit more difficult to deprotonate the surface of C_3S than our hypothesis $C_3S = C_2S + CaO$ does assume. This might be explained by a lower deprotonation of silicates on C_3S due to the vicinal presence of hydroxides. The main difference in $\Delta_rG° - \Delta_dG°$ for C_3S comes from the "CaO part" which is far from to be fully deprotonated as supposed in the former

Table 6
Set of parameters used for the fit of the β-C_2S.

A_1	−17.32	A_2	−0.72	ln Π_b	−51
B_1	2.33E−06	B_2	7.92E−03		
$X0_1$	−54.90	$X0_2$	−44.49		
d_1	1.37	d_2	0.99		

Table 7
Free enthalpies of dissolution related to the reaction of Ca_3SiO_5, Ca_2SiO_4 and CaO respectively with water.

	Vm	$\Delta_rG°$	$\Delta_dG°$ (exp)	$\Delta_rG° - \Delta_dG°$ (exp)
	Cm^3/mol	kJ/mol	kJ/mol	kJ/mol
Ca_3SiO_5	71.0	56.8	125.7	68.9
Ca_2SiO_4	52.0	95.7	99.2	3.5
CaO	17.0	−27.8	28.8	56.6
$C_3S - (C_2S + CaO)$				8.7

thermodynamic calculations. The strong similarity between C_3S and $CaO + C_2S$ supports our assumption that the superficial hydroxylation is a prime phenomenon. The correct solubility equilibriums are actually between the hydroxylated species at the mineral/water interface and the species in solution.

5.3. Extension of the dissolution law to concentrated systems and cements

The interest of tricalcium silicate is to be the main anhydrous phase in Portland cement, therefore it is predestined to be used in concentrated pastes in order to form a binder material. In pure tricalcium silicate pastes and even more in cement pastes, the dissolution of tricalcium silicate occurs simultaneously with the dissolution and precipitation of other phases. This makes monitoring the dissolution of the tricalcium silicate more difficult, since the evolution of the concentrations in Ca and Si are not straightforward. In addition, as explained previously, the apparent inconsistency between the calculated solubility product and the very low hydration rate in pastes, has led to the oversimplified hypothesis that a kind of protective layer should hinder the dissolution [20,25,26,48,49]. Despite the fact that this layer has never been observed even with actual state-of-the-art microscopes, this hypothesis is still today defended by one part of the cement field community and still strongly disputed by the other part. Thanks to the dissolution law of this study, we can check whether some additional parameter(s) or law(s) is (are) needed to reproduce the consumption rate of tricalcium silicate observed in tricalcium silicate pastes or in cement.

5.3.1. Dissolution experiments in concentrated suspensions

Avoiding the precipitation of hydrates and carrying out dissolution experiments in concentrated suspensions is quite difficult. Damidot et al. have performed such experiments using a special experimental set-up which minimizes the contact duration between the tricalcium silicate and the solution [34]. In this article, dissolution rates of a tricalcium silicate in various solutions are reported. In her thesis, Garrault [50] shows hydration of C_3S at a liquid to solid ratio of 50 in high concentrations of calcium hydroxide and measured the silicate concentration over the hydration time. During the first minute(s) of contact with water, there was a short period of pure dissolution. It is therefore possible to extract the dissolution rate and to calculate a deviation from equilibrium since the Ca^{2+}, OH^- and silicate concentrations are known. All these data are reported in Table 8 and plotted in Fig. 15 together with our data. Looking at the dissolution rates reported by Damidot and those calculated from Garrault's data, we notice the good agreement with our data for a similar deviation from equilibrium.

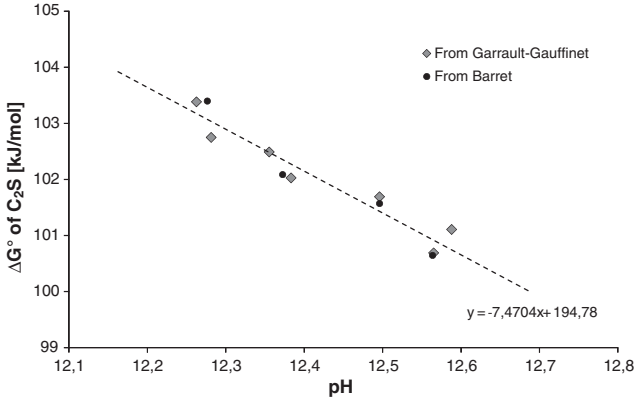

Fig. 13. Variation of the $\Delta G°$ of dissolution for C_2S as a function of pH. Calculated from literature data [44,45].

Even the experiment performed in a saturated calcium hydroxide solution stated incoherent by Damidot et al. is in good agreement according to our study. The apparent discrepancy in Damidot's article comes from neglecting the silicate concentration in their empirical law.

5.3.2. The tricalcium silicate dissolution during its hydration

The hydration of calcium silicates consists of their dissolution accompanied by the precipitation of C–S–H and Portlandite. During hydration, there is no accumulation of ions: the system is at a steady-state between dissolution and precipitation. During this steady-state, the hydration rate is equal to the dissolution rate and to the precipitation rate. Provided that we are able to (1) precisely measure the hydration rate at any given time and (2) determine the tricalcium silicate surface area, we may calculate the interfacial dissolution rates necessary to equal the hydration rate. If ion concentrations are also measured at the same time, we may calculate the ion activity product. There are little data available in the literature where the Ca^{2+}, OH^- and $H_2SiO_4^{2-}$ concentrations have been measured during hydration in paste (water to solid ratio ≤ 1). To the best of our knowledge, there is none in pastes for the tricalcium silicate and only a couple for cement due to the difficulty of extracting the pore solutions when setting and hardening have occurred. We used the numerical values reported in [51]. The degree of hydration of alite has been measured by semi-quantitative XRD and the ion concentrations in pore solution by ICP spectrometry. The relative uncertainty associated with the XRD technique forced us to focus on the time interval between 4 and 10 h to get a confident enough estimation of the instantaneous hydration rate. The hydration rate during this period is equal to the dissolution rate. The surface of alite at this time is estimated knowing the initial specific area. We assume that the initial specific surface area of alite in cement is the same as the cement itself. Then, knowing the mass decrease of alite over time, we calculate the surface decrease assuming spherical particles. With the surface area, we calculate the interfacial dissolution rate. The ion activity product is calculated from the ion concentrations also reported in the article. Results from Lothenbach's data are also shown in Table 8 and plotted in Fig. 15.

In spite of the different origins and polymorphisms of tricalcium silicates, all points are closely together, except far from equilibrium. The dissolution rate law near equilibrium is quite similar for all of them. This law can as well reproduce the dissolution rates of tricalcium silicate or alite in ultra-diluted systems as in concentrated systems without (1) neither the artificial assumption of a diffusion layer nor (2) a solution in equilibrium with metastable C–S–H. As already outlined by Juilland et al., this study further demonstrates the questionable use of invoking the formation of a kind of protective layer to account for the dissolution rate of alite from the very first seconds until few hours of hydration.

5.4. Inputs for hydration modeling

The dissolution kinetics of anhydrous phases was until now the missing part for a complete description of the hydration in the area of cement research. The close relationship between the dissolution interfacial rate and the composition of the solution has been emphasized in this paper and could be at least partially implemented in a more general hydration model. In the following, we will discuss the implications and limitations of such a law in order to get a better description of tricalcium silicate hydration kinetics.

5.4.1. The dissolving surface and dissolving surface area

The dissolution features of tricalcium silicate and its physical characterization have been the subject of recent discussions [18,52] highlighting the interface dissolution profile. The surface of minerals is rarely homogeneous in shape (steps), atomic structure (different crystalline faces), and crystal defects. The surface dissolution features will depend

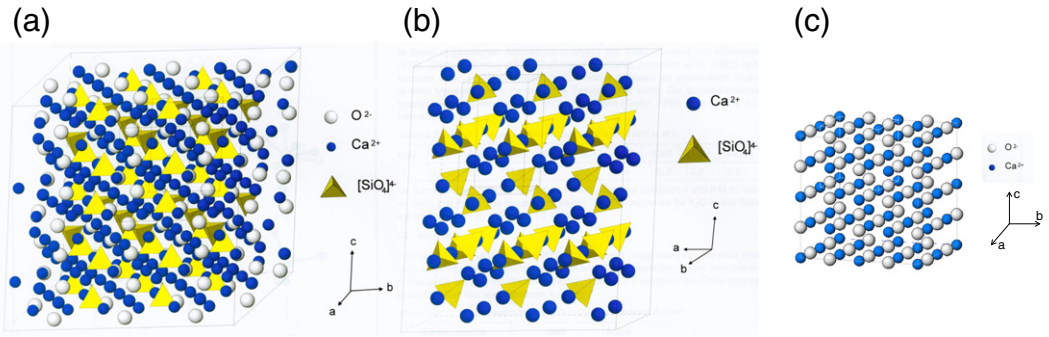

Fig. 14. Crystal structures of (a) triclinic tricalcium silicate (Nishi et al. [46]), (b) monoclinic dicalcium silicate (Jost et al. [47]) and (c) quick lime.

on the type and density of preferential sites (defects). These sites are energetically different, meaning that their potential for dissolution according to an undersaturation state is different. In other words, at high undersaturation a lot of sites can be energetically far enough from the equilibrium to be dissolved; and at low undersaturation only a few are sufficiently undersaturated. When the dissolution of tricalcium silicate occurs in water, pictures obtained from microscopy will tend to show a lot of etch pits at the surface (for instance shown in Fig. 7 of Juilland et al.), whereas it is quite difficult to discern them when the solution is less undersaturated or when the C–S–H have grown and partially covered the grains. Here, it is very important to keep in mind that, for the same mineral, the dissolution surface profile is the consequence of the kinetics (i.e. the undersaturation state), not the opposite. For similar undersaturations, it has been experimentally demonstrated on quartz [53], calcite [54], rutile [55] and many silicates [56], that the number of defects does not play a significant role in the dissolution rate. Blum et al. have shown that the dissolution rate of quartz was only accelerated by a factor of around 2 despite the dislocation density having been increased by a factor of 10^5. This huge increase of dislocations has led to the formation of a multitude of etch pits, highlighting therefore the delicate link between the number of pits and the dissolution kinetics. Lasaga and Lüttge [14,57] proposed that the density defines only how quickly the steady-state is reached and not the steady-state itself. The factor of 2 observed by Blum arose quite accurately from the model thereof. In the field of cement chemistry, some researchers tried to draw conclusions about the role of defects in the early hydration of alite/tricalcium silicate [18,58–63]. The tentative conclusions of these studies was to correlate the length of the low-activity period, observed in the early hydration of C_3S, with the number of defects present in the different tricalcium silicates investigated. All these hydration experiments were carried out in concentrated suspensions, i.e. when C–S–H conjointly precipitated during the dissolution of C_3S. Drawing conclusions on the pure dissolution rate or extrapolating dissolution kinetics without care might be consequently distorted. In the light of the preceding remarks and even having the possibility to get a factor 2 between dissolution rates of a highly defected and an almost free of defect C_3S, it makes more sense to attribute these differences to nucleation of C–S–H. As the nucleation of C–S–H is highly heterogeneous and mainly occurs at the surface of C_3S, the crystal defects present on the surface can also be a factor influencing the number of nuclei and therefore the hydration rate, which is controlled by the nucleation and growth of C–S–H during the first hours [2,64,65]. Interestingly, the dissolution rates reported by Bellmann et al. [63] measured on C_3S samples after various annealing showed relatively minor differences ("lower than the standard deviation of the analytic results"). This observation supports the weak influence of the crystal defect density on the dissolution rate.

The overall dissolution rate is a function of the dissolving surface area. The determination of the exact area which interacts with water during the dissolution is still a difficult problem [66] especially in the differentiation between the total surface area and the reactive one. There are a certain number of issues which have to be considered for properly modeling the surface of dissolution as a function of ΔG:

- The smallest grains have higher total crystal energy than the biggest ones [67] and consequently not exactly the same solubility.
- Small particles are produced during milling and may be flakes of coarser particles. These fragments are usually not spherical. In addition, they present some edges and possess a higher surface energy than the big and round particles.
- The smallest particles are likely to contain more crystal defects which in turn can lead to a variation of $\Delta G_{crit.}$. The sole small particles dissolution causes a rapid decrease of the distance from equilibrium. Assuming a ΔG_{crit} variation, the small particles dissolution can benefit from the opening of etch pits and the big particles do not, which will result in a difference of about one order of magnitude between both dissolution rates.

5.4.2. Modeling of the first exothermal peak obtained by calorimetry

The isothermal calorimetry is commonly used for the determination of the degree of hydration. Although it is a quite efficient and reliable technique as soon as the steady-state is reached, its utilization for the first minutes of hydration is more subject to misunderstandings. Indeed, the apparent discrepancy between the very early dissolution rate and the hydration rate during the first hours [65,68,69] is generally brought to the fore by following the hydration heat of tricalcium silicate or cement by calorimetry. This one shows an intense exothermal peak during the first hour followed by a period of a very low activity. This drop has been inadequately interpreted by the formation of a protective layer. At the first contact with water, the tricalcium silicate will dissolve, and due to the extremely low volume of water present in pastes, this will enrich the solution in Ca^{2+}, OH^- and $H_2SiO_4^{2-}$ extremely fast. Therefore, though being extremely far from equilibrium at the first contact with water, the disequilibrium will be rapidly reduced and the interfacial dissolution rate drops accordingly. In Fig. 16, the evolution of the interfacial dissolution rate is plotted on the left-hand side y-axis assuming a pure dissolution of C_3S at water to solid ratio of 0.5. The dissolution far from equilibrium is so fast and the volume of water so small that the initial burst due to far-from-equilibrium conditions lasts only a couple of milliseconds.

The isothermal calorimeter measures the heat released $\Phi_{th}(t)$ which is, in the first minutes, proportional to the dissolution enthalpy $\Delta_d H$ multiplied by the dissolution rate $R_d(t)$:

$$\Phi_{th}(t) = R_d(t) \cdot \Delta_d H. \quad (26)$$

Table 8
Experimental data from the Literature and the corresponding dissolution rates [34,50,51].

Experimental conditions					Ion concentrations					Ion activities			Rate (μmol/m²/s)
References	Starting Conditions		Liquid to C_3S Ratio	% C_3S dissolved at estimation of the rate	Ca (mM)	Si (mM)	Na or K (mM)	SO_4 (mM)	Cl (mM)	(OH^-)	(Ca^{2+})	(H_4SiO_4)	Ln Π
Ref. Lothenbach	Hydration in cement paste (6h)	20 °C	0.5	16%	22.1	0.06	367	139	0	7.28E−02	2.25E−03	1.41E−08	−52.0876	−0.01
Ref. Lothenbach	Hydration in cement paste (7 h)	20 °C	0.5	32%	21.3	0.07	380	151	0	6.55E−02	2.17E−03	1.95E−08	−52.5157	−0.01
Ref. Garrault	30 first seconds (dissolution step)	25 °C	50	Negligible	20	0.011	0	0	0	2.89E−02	7.37E−03	1.56E−08	−53.9730	−0.13
Ref. Garrault	30 first seconds (dissolution step)	25 °C	50	Negligible	22	0.0098	0	0	0	3.14E−02	7.81E−03	1.24E−08	−53.5372	−0.12
Ref. Garrault	30 first seconds (dissolution step)	25 °C	50	Negligible	33	0.0038	0	0	0	4.42E−02	9.91E−03	2.88E−09	−52.2182	−0.04
Ref. Damidot	Dissolution in water	25 °C	~0.5	Negligible	2.85	0.95	0	0	0	4.16E−03	1.87E−03	1.34E−05	−62.9501	−10.92
Ref. Damidot	Dissolution in 20 mM $CaCl_2$	25 °C	~0.5	Negligible	21.8	0.6	0	0	40	2.06E−03	9.46E−03	1.51E−05	−62.1854	−7.13
Ref. Damidot	Dissolution in 30 mM NaOH	25 °C	~0.5	Negligible	1.23	0.41	30	0	0	2.62E−02	5.09E−04	6.91E−07	−58.7864	−5.04
Ref. Damidot	Dissolution in 22 mM $Ca(OH)_2$	25 °C	~0.5	Negligible	22.2	0.012	0	0	0	3.16E−02	7.86E−03	1.50E−08	−53.2829	−0.05
Ref. Damidot	Dissolution in 5.75 mM $Ca(OH)_2$	25 °C	~0.5	Negligible	6.32	0.19	0	0	0	1.03E−02	3.41E−03	9.91E−07	−58.3291	−2.08

The Φ_m signal delivered by the calorimeter is deformed due to the inertia of the calorimeter and equals to the convolution product of the heat released Φ_{th} and the transfer function T related to the calorimeter:

$$\Phi_m(t) = \Phi_{th}(t) \otimes T(t). \quad (27)$$

The transfer function can be approximated by a sum of exponential decays [70]:

$$T(t) = \sum_i a_i \cdot e^{\left(\frac{-t}{\tau_i}\right)} \quad (28)$$

with a_i the amplitude constants and τ_i the time constants.

For the sake of simplicity, we will assume that the transfer function is a single exponential function and we fixed $a = 0.0007$ and $\tau = 135$ s. These values are chosen to be similar with previous ones measured on a typical calorimeter [71] but the choice does not change the conclusion of the demonstration. The convolution product is calculated with the following algorithm (convolution theorem):

$$\Phi_{th}(t) \otimes T(t) = F^{-1}(F(\Phi_{th}(t)) \cdot F(T(t))) \quad (29)$$

with F and F^{-1} the Fourier transform and the inverse Fourier transform, respectively. We see in Fig. 16 that the convoluted heat measured by the calorimeter is quite broadened in comparison with the extremely sharp dissolution rate peak. The shape of the calculated heat flow curve, based only on the dissolution law, is very similar to typical heat evolution rate curves found in the literature. This result means that it is possible to reproduce the first heat peak revealed during the hydration of tricalcium silicate only with the dissolution kinetics of tricalcium silicate.

5.4.3. The distance from equilibrium during the hydration

This study allows the quantitative comparison of the C_3S and C_2S reactivities. It is well-known that C_2S reacts more slowly than C_3S in ordinary cement paste, which was confirmed experimentally in this study. Indeed, for any concentrations in Ca^{2+}, OH^- and H_4SiO_4 the dissolution rate of C_2S will be lower than the dissolution rate of C_3S. It can also be determined that, for a given concentration of H_4SiO_4, the ratio between the dissolution rates R_{C3S}/R_{C2S} will tend to decrease when the calcium hydroxide concentration also decreases. In other words, this means that the dissolution rate of C_2S will be less disfavored compared to C_3S at low concentration in calcium hydroxide. The C_2S in cement pastes starts to significantly react only many hours after wetting, when the calcium hydroxide concentration in pore solution has also significantly dropped. By using the data of B. Lothenbach, we have calculated the dissolution rates of C_3S and C_2S according to the reported ion concentrations, as well as the ratio between both (see Table 9). The rates calculated are consistent with the Q-XRD data reported. Whereas the system is always undersaturated with respect to C_3S, it is not the case for C_2S between 1 and 6 h. The ion concentrations in solution are strongly controlled by the dissolution of C_3S and the precipitation of C–S–H, which in turn limit the dissolution of C_2S. The latter can only dissolve at the very beginning or after a couple of hours. Looking at the ratio between the rates, the C_3S is always dominating but less and less at low Ca concentrations.

6. Conclusion

Through a specially designed experimental set-up, the dissolution kinetics of tricalcium silicate and dicalcium silicate were measured in conditions free of C–S–H. A clear dependence of the dissolution rates with the degree of disequilibrium was observed. The kinetic laws obtained over a broad range of ion activities enables an extrapolation to rate zero, i.e. at equilibrium, hence the determination of the solubility products. These relative low experimental solubility products

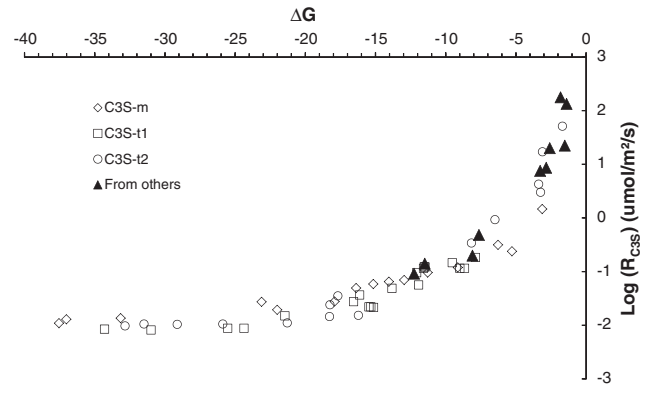

Fig. 15. Dissolution rates of the different tricalcium silicates of this study as well as points obtained from the literature according to the distance from equilibrium. Due to the difference of several orders of magnitude between the rates far from and near equilibrium, a logarithmic scale is proposed.

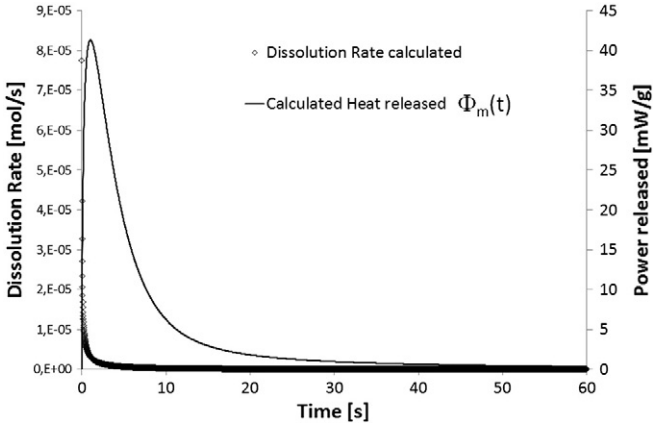

Fig. 16. Evolution of the dissolution rate of 1 g of tricalcium silicate mixed with 0.5 g of water and the corresponding heat flow which could be delivered by any calorimeter.

are the result of equilibrated reactions imposed between the alkaline solution and the hydroxylated surface of C_3S and C_2S.

The switch between the two dissolution mechanisms (step-waves emanating from etch pits and opening of etch pits) proposed by Lasaga and Lüttge has been clearly identified for all samples except for the monoclinic polymorph of C_3S. It does not mean that the switch does not exist for the latter since very high distances from equilibrium might be not maintained for long enough to allow the opening of etch pits in this polymorph.

The original discrepancy between the calculated and experimental solubilities has been resolved without the need for introducing a diffusion barrier onto the C_3S surface. In addition, the dissolution rates of C_3S in more concentrated suspensions and in cement are in good agreement with the kinetic law obtained in diluted suspensions devoid of C–S–H of this study. These two points invalidate the hypothesis of the precipitation of a thin hydrate layer onto the C_3S surface for accounting the dissolution kinetics of C_3S over the entire range of undersaturations in diluted or concentrated systems. The determination of the interfacial dissolution rates of these two anhydrous calcium silicate phases according to the composition of the pore solution should offer the necessary missing part in order to properly model the hydration of these cement phases. The hydration is a dynamic process where the composition of the pore solution varies as well as the surface areas in contact with water. Modeling the evolution of the surface area is the next step for completing a hydration model. That will be the subject of a next article.

Acknowledgment

The authors would like to sincerely thank Barbara Lothenbach and Denis Damidot for making available the original numerical values of their publications and Christophe Labbez for the fruitful discussions.

Appendix A

Table 10
Equilibriums considered in solution or solubility equilibriums used in Phreeqc with the corresponding constants. Only the relevant chemical equilibriums used in this study are listed.

Solubility equilibriums	Log K
$Ca(OH)_2 + 2H^+ \leftrightarrows Ca^{2+} + 2H_2O$	22.88
$SiO_2 + 2H_2O \leftrightarrows H_4SiO_4$	−2.71
$Ca_{0.8}SiO_{5.4}H_{5.2} + 1.6H^+ \leftrightarrows 0.8Ca^{2+} + H_4SiO_4 + 1.4H_2O$	11.12
$Ca_{1.1}SiO_{6.3}H_{6.4} + 2.2H^+ \leftrightarrows 1.1Ca^{2+} + H_4SiO_4 + 2.3H_2O$	16.82
$Ca_{1.8}SiO_{8.4}H_{9.2} + 1.6H^+ \leftrightarrows 1.8Ca^{2+} + H_4SiO_4 + 4.4H_2O$	33.33

Equilibriums in solution	Log K
$H_2O \leftrightarrows OH^- + H^+$	−14
$Na^+ + H_2O \leftrightarrows NaOH + H^+$	−14.18
$H_4SiO_4 \leftrightarrows H_3SiO_4^- + H^+$	−9.83
$H_4SiO_4 \leftrightarrows H_2SiO_4^{2-} + 2H^+$	−23
$Ca^{2+} + SO_4^{2-} \leftrightarrows CaSO_4^\circ$	2.3
$Ca^{2+} + HSO_4^- \leftrightarrows CaHSO_4^+$	1.08
$Na^+ + SO_4^{2-} \leftrightarrows NaSO_4^-$	0.7
$Ca^{2+} + H_2O \leftrightarrows CaOH^+ + H^+$	−12.78

Table 9
Dissolution rates of C_3S and C_2S and ratio between both calculated from values reported in [51].

Time [h]	[Ca]	[Si]	[K + Na]	$[SO_4^{2-}]$	(OH^-)	(Ca^{2+})	(H_4SiO_4)	Diss. rate C_2S	Diss. rate C_3S	Ratio C_3S/C_2S
0.5	21.1	0.1	378	163	5.34E−02	2.27E−03	4.76E−08	−7.48E−04	−0.047	62.6
1	22.2	0.09	388	156	6.80E−02	2.36E−03	2.98E−08	0	−0.020	∞
1.5	22.9	0.07	388	150	7.56E−02	2.43E−03	1.96E−08	0	−0.015	∞
2	24.1	0.06	389	147	8.07E−02	2.55E−03	1.52E−08	0	−0.012	∞
4	23	0.07	387	150	7.51E−02	2.44E−03	1.98E−08	0	−0.015	∞
6	22.1	0.06	367	139	7.60E−02	2.39E−03	1.66E−08	0	−0.018	∞
7	21.3	0.07	380	151	6.85E−02	2.28E−03	2.29E−08	−1.34E−04	−0.026	194.0
16	9.5	0.07	462	136	1.18E−01	9.56E−04	9.61E−09	−1.22E−03	−0.031	25.4
69	2	0.21	529	9	2.90E−01	1.89E−04	5.80E−09	−1.68E−03	−0.030	17.8
144	2.1	0.24	575	10	3.10E−01	1.89E−04	5.90E−09	−7.94E−04	−0.021	26.8
336	1.9	0.23	566	10	3.06E−01	1.73E−04	5.79E−09	−1.56E−03	−0.029	18.4

Table 11
Experiments carried out using the different anhydrous phases C_3S, C_2S and CaO, respectively.

Experimental Conditions					Ion Concentrations				Ion Activities				Rates	
Type of mineral	Starting conditions	T [°C]	Liquid to C_3S ratio	% mineral dissolved at estimation of the rate	Ca (mM)	Si (mM)	Na (mM)	Cl (mM)	$(OH-)$	(Ca^{2+})	(H_4SiO_4)	Ln Π	Rate (g/g/min)	Rate (μmol/m²/s)
C_3S-m	In 200 mM NaCl	20°	10,000	11%	0.141	0.047	200	200	1.57E−04	4.57E−05	9.77E−06	−94.1	0.6210	−114.74
C_3S-m	In 100 mM NaCl	20°	10,000	10%	0.1305	0.0435	100	100	1.63E−04	5.13E−05	9.10E−06	−93.6	0.5080	−93.86
C_3S-m	In 50 mM NaCl	20°	10,000	16%	0.21	0.07	50	50	2.82E−04	9.92E−05	9.66E−06	−88.2	0.4960	−91.64
C_3S-m	In 50 mM NaCl	20°	10,000	17%	0.2226	0.0742	50	50	2.99E−04	1.05E−04	9.74E−06	−87.7	0.4190	−77.42
C_3S-m	In water	20°	10,000	18%	0.2433	0.0811	0	0	4.00E−04	2.14E−04	9.53E−06	−83.8	0.4005	−74.00
C_3S-m	In 1 mM $Ca(OH)_2$	20°	10,000	7%	1.0927	0.0309	0	0	1.99E−03	8.26E−04	7.73E−07	−72.7	0.2794	−51.62
C_3S-m	In 10 mM NaOH	20°	10,000	6%	0.084	0.028	10	0	9.05E−03	4.84E−05	1.41E−07	−73.8	0.1983	−36.64
C_3S-m	In 2 mM $Ca(OH)_2$	20°	10,000	5%	2.1	0.0219	0	0	3.57E−03	1.38E−03	2.98E−07	−68.6	0.1949	−36.01
C_3S-m	In 0.1g C_3S solution	20°	10,000	3%	1.77	0.59	0	0	2.65E−03	1.25E−03	1.09E−05	−67.1	0.1094	−20.22
C_3S-m	In 50 mM NaOH	20°	10,000	3%	0.1289	0.1403	50	0	3.95E−02	3.95E−05	1.07E−07	−65.9	0.0921	−17.02
C_3S-m	In 100 mM NaOH	20°	10,000	3%	0.1269	0.095	100	0	7.28E−02	2.66E−05	2.71E−08	−64.7	0.0834	−15.40
C_3S-m	In 3 mM $Ca(OH)_2$	20°	10,000	3%	3.31	0.1014	0	0	5.61E−03	2.04E−03	8.49E−07	−63.7	0.0777	−14.36
C_3S-m	In 0.2g C_3S	20°	10,000	2%	3.36	1.12	0	0	4.78E−03	2.09E−03	1.11E−05	−62.0	0.0565	−10.44
C_3S-m	In 6 mM $Ca(OH)_2$	20°	10,000	2%	6.12	0.0748	0	0	9.90E−03	3.21E−03	3.31E−07	−59.8	0.0454	−8.39
C_3S-m	In 10 mM $Ca(OH)_2$	20°	10,000	2%	10.1	0.0551	0	0	1.55E−02	4.51E−03	1.43E−07	−57.0	0.0172	−3.18
C_3S-m	In 0.1g C_3S +100 mM NaOH	20°	10,000	6%	1.3857	0.4619	100	0	7.36E−02	2.88E−04	1.29E−07	−56.0	0.0227	−4.19
C_3S-m	In 20 mM $Ca(OH)_2$	20°	10,000	2%	19.81	0.0241	0	0	2.77E−02	6.82E−03	2.91E−08	−53.8	0.0037	−0.68
C_3S-t1	In water	25°	50,000	23%	0.0594	0.0198	0	0	1.05E−04	5.58E−05	7.70E−06	−96.1	0.3830	−127.84
C_3S-t1	In water	25°	10,000	16%	0.2082	0.0694	0	0	3.47E−04	1.85E−04	1.11E−05	−85.0	0.3557	−118.73
C_3S-t1	In water	25°	10,000	25%	0.304	0.1099	0	0	4.92E−04	2.64E−04	1.29E−05	−81.7	0.3694	−123.30
C_3S-t1	In 1 mM $Ca(OH)_2$	25°	10,000	1%	0.89	0.003	0	0	1.66E−03	6.97E−04	1.12E−07	−76.2	0.3420	−114.15
C_3S-t1	In 0.5 mM $Ca(OH)_2$	25°	10,000	18%	0.6976	0.0787	0	0	1.24E−03	5.62E−04	3.85E−06	−75.1	0.3420	−114.15
C_3S-t1	In 1 mM $Ca(OH)_2$	25°	10,000	9%	1.0961	0.0413	0	0	1.99E−03	8.37E−04	1.26E−06	−72.1	0.2011	−67.12
C_3S-t1	In 2.5 mM $Ca(OH)_2$	25°	50,000	11%	2.6	0.01	0	0	4.60E−03	1.73E−03	1.28E−07	−67.3	0.1094	−36.52
C_3S-t1	In 2.5 mM $Ca(OH)_2$	25°	10,000	3%	2.69	0.012	0	0	4.75E−03	1.77E−03	1.48E−07	−66.8	0.0821	−27.40
C_3S-t1	In 2.5 mM $Ca(OH)_2$	25°	10,000	5%	2.7	0.023	0	0	4.75E−03	1.78E−03	2.84E−07	−66.2	0.1368	−45.66
C_3S-t1	In 2.5 mM $Ca(OH)_2$	25°	10,000	6%	2.6887	0.0273	0	0	4.73E−03	1.77E−03	3.38E−07	−66.0	0.1368	−45.66
C_3S-t1	In 2.75 mM $Ca(OH)_2$	25°	10,000	9%	2.64	0.038	0	0	4.64E−03	1.75E−03	4.81E−07	−65.8	0.1399	−46.70
C_3S-t1	In 5 mM $Ca(OH)_2$	25°	50,000	2%	5	0.0017	0	0	8.45E−03	2.87E−03	1.11E−08	−64.5	0.0616	−20.56
C_3S-t1	In 5 mM $Ca(OH)_2$	25°	10,000	1%	5.54	0.005	0	0	9.27E−03	3.10E−03	2.94E−08	−62.8	0.0315	−10.51
C_3S-t1	In 5 mM $Ca(OH)_2$	25°	10,000	1%	5.5	0.006	0	0	9.21E−03	3.08E−03	3.56E−08	−62.6	0.0534	−17.82
C_3S-t1	In 5.5 mM $Ca(OH)_2$	25°	10,000	2%	5.52	0.0083	0	0	9.24E−03	3.09E−03	4.92E−08	−62.3	0.0260	−8.68
C_3S-t1	In 5 mM $Ca(OH)_2$	25°	10,000	2%	5.5	0.009	0	0	9.21E−03	3.08E−03	5.34E−08	−62.2	0.0245	−8.18
C_3S-t1	In 5.5 mM $Ca(OH)_2$	25°	10,000	2%	5.4795	0.0098	0	0	9.17E−03	3.07E−03	5.84E−08	−62.2	0.0246	−8.21
C_3S-t1	In 8.5 mM $Ca(OH)_2$	25°	50,000	1%	8.5	0.0011	0	0	1.59E−02	4.73E−03	4.11E−09	−60.2	0.0205	−6.84
C_3S-t1	In 8.5 mM $Ca(OH)_2$	25°	10,000	2%	8.43	0.007	0	0	1.35E−02	4.19E−03	2.64E−08	−59.7	0.0260	−8.68
C_3S-t1	In 8.5 mM $Ca(OH)_2$	25°	10,000	2%	8.4	0.01	0	0	1.35E−02	4.18E−03	3.79E−08	−59.4	0.0260	−8.68
C_3S-t1	In 10.5 mM $Ca(OH)_2$	25°	10,000	1%	10.6	0.005	0	0	1.66E−02	4.90E−03	1.47E−08	−58.6	0.0164	−5.47
C_3S-t2	In water	25°	10,000	19%	0.246	0.082	0	0	4.07E−04	2.17E−04	1.14E−05	−83.5	0.5267	−103.22
C_3S-t2	In water	25°	10,000	22%	0.2874	0.0958	0	0	4.72E−04	2.50E−04	1.17E−05	−82.2	0.4856	−95.17
C_3S-t2	In water	25°	10,000	29%	0.3777	0.1259	0	0	6.14E−04	3.23E−04	1.21E−05	−79.8	0.4925	−96.52
C_3S-t2	In 9 mM $CaCl_2$	25°	10,000	15%	9.25	0.066	0	18.104	2.68E−04	5.05E−03	1.17E−05	−76.6	0.4856	−95.17
C_3S-t2	In 13 mM $CaCl_2$	25°	10,000	30%	13	0.13	0	25.22	4.96E−04	6.53E−03	1.33E−05	−72.0	0.4638	−90.89
C_3S-t2	In C_3S dissolved solution	25°	10,000	~1%	1.3627	0.4382	0	0	2.10E−03	1.01E−03	1.23E−05	−69.0	0.3529	−69.16
C_3S-t2	In 22 mM NaOH	25°	10,000	8%	0.138	0.034	22	0	1.89E−02	6.57E−05	8.78E−08	−68.9	0.2120	−41.55
C_3S-t2	In 32 mM NaOH	25°	10,000	7%	0.118	0.029	32	0	2.67E−02	4.90E−05	4.80E−08	−68.4	0.1450	−28.42
C_3S-t2	In C_3S dissolved solution	25°	10,000	~1%	1.7459	0.5476	0	0	2.67E−03	1.25E−03	1.23E−05	−66.9	0.3338	−65.42
C_3S-t2	In 11 mM $Ca(OH)_2$	25°	10,000	1%	11	0.003	0	0	1.72E−02	5.02E−03	8.46E−09	−58.9	0.0150	−2.94
C_3S-t2	In 15 mM $Ca(OH)_2$	25°	10,000	1%	15	0.0024	0	0	2.25E−02	6.15E−03	4.77E−09	−57.2	0.0055	−1.08
C_3S-t2	In C_3S solution hydrated and filtrated	25°	10,000	<1%	21	7.5	0	0	3.01E−02	7.59E−03	1.00E−08	−54.1	0.0012	−0.24
C_3S-t2	In C_3S solution hydrated and filtrated	25°	10,000	<1%	21	8.6	0	0	3.01E−02	7.59E−03	1.15E−08	−53.9	0.0017	−0.33
C_3S-t2	In C_3S solution hydrated and filtrated	25°	10,000	<1%	20	13	0	0	2.89E−02	7.37E−03	1.84E−08	−53.8	0.0003	−0.06

Table 11 (*continued*)

Experimental Conditions					Ion Concentrations				Ion Activities				Rates	
Type of mineral	Starting conditions	T [°C]	Liquid to C_3S ratio	% mineral dissolved at estimation of the rate	Ca (mM)	Si (mM)	Na (mM)	Cl (mM)	(OH−)	(Ca^{2+})	(H_4SiO_4)	Ln Π	Rate (g/g/min)	Rate (μmol/m^2/s)
C_3S-t2	In C_3S solution hydrated and filtrated	25°	10,000	<1%	25	15	0	0	3.50E−02	8.44E−03	1.62E−08	−52.4	0.0001	−0.02
β-C_2S	In water	20°	10,000	~11%	0.0254	0.0127	0	0	4.46E−05	2.44E−05	6.99E−06	−73.2	0.5570	−18.40
β-C_2S	In 200 mM NaCl	20°	10,000	~8%	0.085	0.0425	200	200	9.05E−05	2.76E−05	1.34E−05	−69.5	0.5100	−16.84
β-C_2S	In 100 mM NaCl	20°	10,000	~8%	0.0974	0.0487	100	100	1.15E−04	3.83E−05	1.33E−05	−67.9	0.5288	−17.46
β-C_2S	In water	20°	10,000	~6%	0.0948	0.0474	0	0	1.51E−04	8.75E−05	1.25E−05	−65.2	0.5082	−16.78
β-C_2S	In 1 mM $Ca(OH)_2$	20°	10,000	~4%	1.0436	0.0218	0	0	1.91E−03	7.94E−04	5.68E−07	−53.7	0.1545	−5.10
β-C_2S	In 50 mM NaOH	20°	10,000	~2.5%	0.0416	0.0208	50	0	3.95E−02	1.28E−05	1.58E−08	−53.4	0.1070	−3.53
β-C_2S	In 100 mM NaOH	20°	10,000	~3%	0.038	0.019	100	0	7.28E−02	7.98E−06	5.42E−09	−53.0	0.0992	−3.28
β-C_2S	In 200 mM NaOH	20°	10,000	~1.6%	0.0186	0.0093	200	0	1.31E−01	2.56E−06	9.07E−09	−52.4	0.0700	−2.31
β-C_2S	In 6 mM $Ca(OH)_2$	20°	10,000	~0.5%	6.41	0.0027	0	0	1.04E−02	3.32E−03	1.15E−07	−45.7	0.0172	−0.57
β-C_2S	In 11 mM $Ca(OH)_2$	20°	10,000	~0.4%	11.1	0.0022	0	0	1.68E−02	4.79E−03	5.13E−08	−43.8	0.0077	−0.25
β-C_2S	In 14 mM $Ca(OH)_2$	20°	10,000	~0.1%	14.1	0.0016	0	0	2.07E−02	5.57E−03	2.79E−08	−43.3	0.0039	−0.13
β-C_2S	In 17 mM $Ca(OH)_2$	20°	10,000	~0.1%	16.97	0.0015	0	0	2.43E−02	6.23E−03	2.13E−08	−42.7	0.0029	−0.09
β-C_2S	In 20 mM $Ca(OH)_2$	20°	10,000	~0.1%	21.46	0.0012	0	0	2.97E−02	7.15E−03	1.30E−08	−42.1	0.0016	−0.05
CaO	In water	20°	10,000	24.7%	0.44	0	0	0	8.38E-04	3.69E−04		−22.1	−6.32	
CaO	In CaO solution	20°	10,000	25.5%	2.06	0	0	0	3.67E-03	1.40E−03		−17.8	−6.44	
CaO	In CaO solution	20°	10,000	19.6%	3.89	0	0	0	6.61E−03	2.31E−03		−16.1	−6.08	
CaO	In CaO solution	20°	10,000	26.4%	9.16	0	0	0	1.43E−02	4.23E−03		−14.0	−5.40	
CaO	In CaO solution	20°	10,000	20.4%	11.6	0	0	0	1.75E−02	4.93E−03		−13.4	−5.08	
CaO	In CaO solution	20°	10,000	18.8%	13.1	0	0	0	1.95E−02	5.32E−03		−13.1	−3.25	
CaO	In 18 mM $Ca(OH)_2$	20°	2000	19.1%	19.8	0	0	0	2.77E−02	6.82E−03		−12.2	−2.07	
CaO	In 24 mM $Ca(OH)_2$	20°	10,000	39.0%	24.7	0	0	0	3.34E−02	7.73E−03		−11.7	−0.04	
CaO	In 0.01M KOH	20°	10,000	25.7%	0.458	0	10	0	9.68E−03	2.58E−04		−17.5	−4.34	
CaO	In 0.1M KOH	20°	10,000	21.7%	0.386	0	100	0	7.48E−02	7.95E−05		−14.6	−1.71	
CaO	In 0.3M KOH	20°	10,000	21.4%	0.382	0	300	0	1.93E−01	3.92E−05		−13.4	−0.56	
CaO	In 0.01M NaOH	20°	10,000	19.5%	0.348	0	10	0	9.48E−03	1.97E−04		−17.8	−3.75	
CaO	In 0.1M NaOH	20°	10,000	21.9%	0.39	0	100	0	7.32E−02	8.16E−05		−14.6	−1.67	
CaO	In 0.1M NaOH	20°	10,000	21.0%	0.375	0	100	0	7.31E−02	7.84E−05		−14.7	−1.24	
CaO	In 0.2M NaOH	20°	10,000	21.8%	0.388	0	200	0	1.31E−01	5.33E−05		−13.9	−1.05	
CaO	In 0.3M NaOH	20°	10,000	21.0%	0.387	0	300	0	1.84E−01	4.12E−05		−13.5	−0.78	
CaO	In 0.5M NaOH	20°	10,000	21.8%	0.389	0	500	0	2.76E−01	3.02E−05		−13.0	−0.45	
CaO	In 1M NaOH	20°	10,000	34.0%	0.575	0	1000	0	4.72E−01	3.01E−05		−11.9	−0.14	
CaO	solubility CaO experimental	20°			25.2	0	0	0	3.40E−02	7.82E−03		−11.6	0	
$Ca(OH)_2$	solubility $Ca(OH)_2$ theoretical	20°			24.48	0	0	0	3.32E−02	7.70E−03		−11.7		
$Ca(OH)_2$	Solubility $Ca(OH)_2$ experimental	20°			24.45	0	0	0	3.31E−02	7.69E−03		−11.7		

References

[1] H.F.W. Taylor, Cement Chemistry 2nd edition, Thomas Telford edition, 1997.
[2] J.J. Thomas, A new approach to modeling the nucleation and growth kinetics of tricalcium silicate hydration, J. Am. Soc. 90 (2007) 311–316.
[3] S. Bishnoi, K. Scrivener, Studying nucleation and growth kinetics of alite hydration using μic, Cem. Concr. Res. 39 (2009) 849–860.
[4] S. Garrault, A. Nonat, Hydrated layer formation on tricalcium and dicalcium silicate surfaces: experimental study and numerical simulations, Langmuir 17 (2001) 8313–8138.
[5] G.W. Scherer, J. Zhang, J.J. Thomas, Nucleation and growth models for hydration of cement, Cem. Concr. Res. 42 (7) (2012) 982–993.
[6] L. Nicoleau, A. Nonat, A reply to the discussion "Accelerated growth of calcium silicate hydrates: experiments and simulations", Cem. Concr. Res. 42 (6) (2012) 881–887.
[7] T.E. Burch, K.L. Nagy, A.C. Lasaga, Free energy dependence of albite dissolution kinetics at 80 °C and pH = 8.8, Chem. Geol. 105 (1993) 137–162.
[8] K.L. Nagy, A. Lasaga, Dissolution and precipitation kinetics of gibbsite at 80 °C and pH = 3: the dependence on solution saturation state, Geochim. Cosmochim. Acta 56 (1992) 3093–3111.
[9] A.S. Taylor, J.D. Blum, A.C. Lasaga, The dependence of labradorite dissolution and Sr isotope release rates on solution saturation state, Geochim. Cosmochim. Acta 64 (14) (2000) 2389–2400.
[10] J. Cama, J. Ganor, C. Ayora, A.C. Lasaga, Smectite dissolution kinetics at 80 °C and pH = 8.8, Geochim. Cosmochim. Acta 64 (15) (2000) 2701–2717.
[11] K.L. Nagy, A.E. Blum, A.C. Lasaga, Dissolution and precipitation kinetics of kaolinite at 80 °C and pH = 3; the dependence on solution saturation state, Am. J. Sci. 1 (291) (1991) 649–686.
[12] A.C. Lasaga, Transition State Theory in Kinetics of Geochemical Processes, vol. 8, 1981. (ISBN13 978-0-939950-08-9).
[13] P. Aagaard, H.C. Helgeson, Thermodynamic and kinetic constraints on reaction rates among minerals and aqueous solutions—I. Theoretical considerations, Am. J. Sci. 282 (1982) 237–285.
[14] A.C. Lasaga, A. Lüttge, A model for crystal dissolution, Eur. J. Mineral. 15 (2003) 603–615.
[15] A. Lüttge, Crystal dissolution kinetics and Gibbs free energy, J. Electron Spectrosc. Relat. Phenom. 150 (2006) 248–259.
[16] T.E. Burch, K.L. Nagy, A.C. Lasaga, Free energy of albite dissolution kinetics at 80 °C and pH 8.8, Chem. Geol. 105 (1993) 137–162.
[17] L. Nicoleau, Interactions physico-chimiques entre les latex et les phases minérales constituant le ciment au cours de l'hydratation, Ph-D thesis, University of Burgundy, 2004, Dijon (France).
[18] P. Juilland, E. Gallucci, R. Flatt, K. Scrivener, Dissolution theory applied to the induction period in alite hydration, Cem. Concr. Res. 40 (2010) 831–844.
[19] E. Gartner, Discussion of the paper "Dissolution theory applied to the induction period in alite hydration" by Juilland et al. Cem. Concr. Res. 41 (5) (2011) 560–562.
[20] F. Bellmann, D. Damidot, B. Möser, J. Skibsted, Improved evidence for the existence of an intermediate phase during hydration of tricalcium silicate, Cem. Concr. Res. 40 (6) (2010) 875–884.
[21] R.A. Livingston, N.M. Nemes, D.A. Neumann, Quasi-elastic neutron scattering investigation of the effect of water/cement ratio on tricalcium silicate hydration, Proceedings of 11th ICCC, 2011, (Madrid (Spain)).
[22] J.W. Bullard, et al., Mechanisms of cement hydration, Cem. Concr. Res. 41 (12) (2011) 1208–1223.
[23] J.J. Chen, J.J. Thomas, H.F.W. Taylor, H.M. Jennings, Solubility and structure of calcium silicate hydrate, Cem. Concr. Res. 34 (2004) 1499–1519.
[24] A.A. Jeschke, W. Dreybrodt, Dissolution rates of minerals and their relation to surface morphology, Geochim. Cosmochim. Acta 66 (17) (2002) 3055–3062.
[25] H.N. Stein, J.M. Stevels, Influence of silica on the hydration of 3CaO, SiO_2, J. Appl. Chem. 14 (1964) 338–346.
[26] E.M. Gartner, H.M. Jennings, Thermodynamics of calcium silicate hydrates and their solutions, J. Am. Ceram. Soc. 70 (10) (1987) 743–749.
[27] M.W. Chase Jr., NIST-JANAF Thermochemical Tables, Fourth ed., J. Phys. Chem. Ref. Data, Monograph, 9, 1998, pp. 1–1951.

[28] Handbook of Chemistry and Physics 85th edition, D.R. Lide, CRC editions, 2003, Boca Raton.
[29] J.D. Rimstidt, Quartz solubility at low temperatures, Geochim. Cosmochim. Acta 61 (13) (1997) 2553–2558.
[30] V.J. Babushkin, G.M. Matveev, O.P. Mcedlov-Petrosjan, Thermodynamics of Silicates, Springer Verlag Berlin, Moscow, 1986.
[31] I. Gunnarsson, S. Arnorsson, Amorphous silica solubility and the thermodynamic properties of $H_4SiO_4°$ in the range of 0° to 350 °C at P_{sat}, Geochim. Cosmochim. Acta 64 (13) (2000) 2295–2307.
[32] P. Barret, Sur l'existence d'un stade d'hydroxylation superficielle dans le processus de dissolution du silicate tricalcique 3CaO, SiO_2 et son influence sur la solubilité du ciment, C. R. Acad. Sci. Paris t.288 (1979) C-461.
[33] B.C. Hancock, M. Parks, What is the true solubility advantage for amorphous pharmaceuticals, Pharm. Res. 17 (4) (2000) 397–404.
[34] D. Damidot, F. Bellmann, B. Möser, T. Sovoidnich, Modeling of the effect of electrolytes on the rate of early hydration of tricalcium silicate, Proceedings of the 1st Conference on Microstructure Related Durability of Cementitious Composites, RILEM Publications, Nanjing, China, 2008.
[35] A. Nonat, Modelling hydration and setting of cement, Ceramics 92 (2005) 247–257.
[36] I.M. Ritchie, X. Bing-An, The kinetics of lime slaking, Hydrometallurgy 23 (1990) 377–396.
[37] A.C. Lasaga, Fundamental approaches in describing mineral dissolution and precipitation rates, Rev. Mineral. Geochem. 31 (1995) 23–86.
[38] R.O. James, G.A. Parks, Characterization of aqueous colloids by their electrical double-layer and intrinsic surface chemical properties, in: E. Matijevic (Ed.), Surface and Colloid Science, vol. 12, Plenum Press, Springer US, 1982, pp. 119–216.
[39] G. Sposito, On the surface complexation model of the oxide–aqueous solution interface, J. Colloid Interface Sci. 91 (2) (1984) 329–340.
[40] J.A. Davis, D.B. Kent, Surface complexation modeling in aqueous geochemistry, in: M.F. Hochella Jr., A.F. White (Eds.), Mineral–Water Interface Geochemistry, Mineral. Soc. Amer, 1990, pp. 177–259.
[41] D.A. Dzomak, F.M.M. Morel, Surface Complexation Modeling, Wiley, 1990.
[42] P.M. Dove, The dissolution kinetics of quartz in sodium chloride solutions at 25 °C to 300 °C, Am. J. Sci. 294 (1994) 665–712.
[43] W. Vogelsberger, M. Löbbus, J. Sonnefeld, A. Seidel, The influence of ionic strength on the dissolution process of silica, Colloids Surf., A Physicochem. Eng. Asp. 159 (1999) 311–319.
[44] P. Barret, D. Bertrandie, Saturated solutions of anhydrous phases in the system lime–silica–water: example of β-C_2S, J. Am. Ceram. Soc. 73 (11) (1990) 3486–3492.
[45] S. Garrault-Gauffinet, A. Nonat, Experimental investigation of calcium silicate hydrate (C–S–H) nucleation, J. Cryst. Growth 200 (1999) 565–574.
[46] F. Nishi, Y. Takéuchi, Tricalcium silicate $Ca_3O[SiO_4]$: the monoclinic superstructure, Z. Kristallogr. 172 (1985) 297–314.
[47] K.H. Jost, B. Ziemer, R. Seydel, Redetermination of the structure of β-dicalcium silicate, Acta Crystallogr. B33 (1977) 1696–1700.
[48] D.L. Kantro, S. Brunauer, C.H. Weise, Development of surface in the hydration of calcium silicates. II. Extension of investigations to earlier and later stages of hydration, J. Phys. Chem. 66 (10) (1962) 1804–1809.
[49] E.M. Gartner, J.M. Gaidis, Hydration mechanisms, The Materials Science of Concrete, I, American Ceramic Society, 1989, pp. 95–125.
[50] S. Garrault-Gauffinet, Etude expérimentale et par simulation numérique de la cinétique de croissance et de la structure des hydrosilicates de calcium, produits d'hydratation des silicates tricalcique et dicalcique, Ph-D Thesis of the Université de Bourgogne, 1998, Dijon (France)
[51] B. Lothenbach, F. Winnefeld, Thermodynamic modeling of the hydration of Portland cement, Cem. Concr. Res. 36 (2006) 209–226.
[52] J.M. Makar, J.J. Beaudoin, T. Sato, R. Alizadeh, L. Raki, Discussion of "Dissolution theory applied to the induction period in alite hydration", Cem. Concr. Res. 41 (5) (2011) 565–567.
[53] A.E. Blum, R.A. Yund, A.C. Lasaga, The effect of dislocation density on the dissolution of quartz,1990, Geochim. Cosmochim. Acta 54 (1990) 283–297.
[54] J. Schott, S. Branley, D. Crerar, C. Gu, M. Borcsik, C. Willaime, Dissolution kinetics of strained calcite, Geochim. Cosmochim. Acta 53 (1989) 373–382.
[55] W.H. Casey, M.J. Carr, R.A. Graham, Crystal defects and the dissolution of rutile, Geochim. Cosmochim. Acta 52 (1988) 1345–1556.
[56] R.T. Cygan, W.H. Casey, M.B. Boslough, H.R. Westrich, M.J. Carr, G.R. Holdren, Dissolution kinetics of experimentally shocked silicate minerals, Chem. Geol. 78 (1989) 229–244.
[57] A.C. Lasaga, A. Lüttge, Variation of crystal dissolution rate based on a dissolution stepwave model, Science 291 (2001) 2400–2404.
[58] I. Odler, J. Schüppstuhl, Early hydration of tricalcium silicate. III. Control of the induction period, Cem. Concr. Res. 11 (1981) 765–774.
[59] T. Sakurai, T. Sato, A. Yoshinaga, 5th ISCC, vol. 1, 1969, pp. 300–321.
[60] J.N. Maycock, J. Skalny, R. Kalyoncu, Crystal defects and hydration. I. Influence of lattice defects, Cem. Concr. Res. 4 (1974) 835–847.
[61] P. Fierens, J.P. Verhaegen, Hydration of tricalcium silicate in paste — kinetics of calcium ions dissolution in the aqueous phase, Cem. Concr. Res. 6 (1976) 337–342.
[62] M. Costoya, Effect of particle size on the hydration kinetics and microstructural development of tricalcium silicate, Ph-D Thesis of the E.P.F.L. no. 4102, 2008, Lausanne (Switzerland).
[63] F. Bellmann, T. Sowoidnich, B. Möser, Formation of an intermediate phase and influence of crystallographic defects on dissolution of C_3S, Proceedings of 13th ICCC, Instituto de Ciencias de la Construccion "eduardo Torroja", Madrid, Spain, 2011.
[64] A. Nonat, S. Garrault, L. Nicoleau, Tricalcium silicate hydration modeling and numerical simulations, Proceedings of CONMOD, 10, 2010, pp. 91–94.
[65] J.W. Bullard, A determination of hydration mechanisms for tricalcium silicate using a kinetic cellular automaton model, J. Am. Ceram. Soc. 91 (7) (2008) 2088–2097.
[66] J.-M. Gautier, E.H. Oelkers, J. Schott, Are quartz dissolution rates proportional to B.E.T. surface areas? Geochim. Cosmochim. Acta 65 (7) (2001) 1059–1070.
[67] A. Navrotsky, Nanoscale effects on thermodynamics and phase equilibria in oxide systems, ChemPhysChem 12 (12) (2011) 2207–2215.
[68] K.G. McCurdy, H.N. Stein, Suspension hydration of C_3S at constant pH. I. Variation of particle size and C_3S content, Cem. Concr. Res. 3 (1973) 247–262.
[69] P.W. Brown, J. Pommerscheim, G. Frohnsdorff, A kinetic model for the hydration of tricalcium silicate, Cem. Concr. Res. 15 (1985) 35–41.
[70] B.G. Lipták, Instruments Engineers' Handbook: Process Control and Optimization, 4th ed., CRC Press, 2006. (Taylor & Francis).
[71] M. Domenech, Chimio-mécanique de l'hydratation du plâtre. Conséquences de l'adjuvantation, Ph-D thesis of the University of Burgundy, 2000, Dijon (France).